

U.S.N.A. --- Trident Scholar project report; no. 325 (2004)

Evaluation of Dynamic Lift Coefficients of High Aspect Ratio Rudders and Control Surfaces

by

Midshipman Jared R. Patton, Class of 2004
United States Naval Academy
Annapolis, Maryland

Certification of Adviser Approval

Assistant Professor Paul H. Miller
Naval Architecture and Ocean Engineering Department

Acceptance for the Trident Scholar Committee

Professor Joyce E. Shade
Deputy Director of Research & Scholarship

REPORT DOCUMENTATION PAGE

Form Approved
OMB No. 074-0188

Public reporting burden for this collection of information is estimated to average 1 hour per response, including the time for reviewing instructions, searching existing data sources, gathering and maintaining the data needed, and completing and reviewing the collection of information. Send comments regarding this burden estimate or any other aspect of the collection of information, including suggestions for reducing this burden to Washington Headquarters Services, Directorate for Information Operations and Reports, 1215 Jefferson Davis Highway, Suite 1204, Arlington, VA 22202-4302, and to the Office of Management and Budget, Paperwork Reduction Project (0704-0188), Washington, DC 20503.

1. AGENCY USE ONLY (Leave blank)		2. REPORT DATE 6 May 2004	3. REPORT TYPE AND DATE COVERED	
4. TITLE AND SUBTITLE Evaluation of dynamic lift coefficients of high aspect ratio rudders and control surfaces			5. FUNDING NUMBERS	
6. AUTHOR(S) Patton, Jared R. (Jared Ryan), 1982-				
7. PERFORMING ORGANIZATION NAME(S) AND ADDRESS(ES)			8. PERFORMING ORGANIZATION REPORT NUMBER	
9. SPONSORING/MONITORING AGENCY NAME(S) AND ADDRESS(ES) US Naval Academy Annapolis, MD 21402			10. SPONSORING/MONITORING AGENCY REPORT NUMBER Trident Scholar project report no. 325 (2004)	
11. SUPPLEMENTARY NOTES				
12a. DISTRIBUTION/AVAILABILITY STATEMENT This document has been approved for public release; its distribution is UNLIMITED.			12b. DISTRIBUTION CODE	
13. ABSTRACT: The goal of this Trident Project was the determination of the maximum dynamic lift coefficient of high aspect ratio control surfaces to reduce the uncertainty in design. The effective design of rudders, diving planes and other control surfaces with high aspect ratios, i.e. a larger depth in proportion to chord length, is hindered by uncertainty in the dynamic coefficient of lift of the control surface as it passes through a transient fluid flow affected by the fluid free surface. This unsteady flow creates momentary spikes in loading, which if large enough, can cause immediate or fatigue-induced failure. High aspect ratio control surfaces are more efficient (higher lift-to-drag ratios) than traditional designs and generate greater lift at smaller angles of attack to the incoming flow, however their increasing length produces significantly greater bending moments in the shaft. This has led to a number of in-service failures. As high aspect ratio lifting surfaces become more commonplace on surface vessels and submarines, more precise knowledge of loading conditions is required to avoid more failures. The dynamic lift coefficient is a dimensionless load factor that can be applied to geometrically similar bodies. As the dynamic coefficient of lift is dimensionless, by employing the principles of similitude, the testing of large bodies such as ships hulls or wing sections can be successfully analyzed through the use of scale models tested in wind tunnels or tow tanks. Data collection took place in the David Taylor Model Basin at the Naval Surface Warfare Center. Two 1/5-scale rudders were tested on a donated 15-foot vessel model. Strain gages were attached to the rudder and shaft to determine the strain distribution and overall deformation. A finite element model of the rudder and shaft correlated the measured strains to hydrodynamic pressures, which led to a determination of the resulting dynamic lift coefficients for various load cases. These were compared to computational fluid dynamics predictions of pressure plots for the same loading. Load cases included constant speed in still water, turning and response in waves. As a result of this project, engineers will have a better understanding of the peak loads on control surfaces, leading to safer and more efficient designs.				
14. SUBJECT TERMS: dynamics ; lift coefficient ; computational fluid dynamics ; finite element analysis ; tow tank testing			15. NUMBER OF PAGES 73	
			16. PRICE CODE	
17. SECURITY CLASSIFICATION OF REPORT	18. SECURITY CLASSIFICATION OF THIS PAGE	19. SECURITY CLASSIFICATION OF ABSTRACT	20. LIMITATION OF ABSTRACT	

ABSTRACT

The goal of this Trident Project was the determination of the maximum dynamic lift coefficient of high aspect ratio control surfaces to reduce the uncertainty in design. The effective design of rudders, diving planes and other control surfaces with high aspect ratios, i.e. a larger depth in proportion to chord length, is hindered by uncertainty in the dynamic coefficient of lift of the control surface as it passes through a transient fluid flow affected by the fluid free surface. This unsteady flow creates momentary spikes in loading, which if large enough, can cause immediate or fatigue-induced failure. High aspect ratio control surfaces are more efficient (higher lift-to-drag ratios) than traditional designs and generate greater lift at smaller angles of attack to the incoming flow, however their increasing length produces significantly greater bending moments in the shaft. This has led to a number of in-service failures. As high aspect ratio lifting surfaces become more commonplace on surface vessels and submarines, more precise knowledge of loading conditions is required to avoid more failures.

The dynamic lift coefficient is a dimensionless load factor that can be applied to geometrically similar bodies. As the dynamic coefficient of lift is dimensionless, by employing the principles of similitude, the testing of large bodies such as ships hulls or wing sections can be successfully analyzed through the use of scale models tested in wind tunnels or tow tanks.

Data collection took place in the David Taylor Model Basin at the Naval Surface Warfare Center. Two 1/5-scale rudders were tested on a donated 15-foot vessel model. Strain gages were attached to the rudder and shaft to determine the strain distribution and overall deformation. A finite element model of the rudder and shaft correlated the measured strains to hydrodynamic pressures, which led to a determination of the resulting dynamic lift coefficients for various load cases. These were compared to computational fluid dynamics predictions of pressure plots for the same loading. Load cases included constant speed in still water, turning and response in waves. As a result of this project, engineers will have a better understanding of the peak loads on control surfaces, leading to safer and more efficient designs.

Keywords: dynamics
lift coefficient
computational fluid dynamics
finite element analysis
tow tank testing

ACKNOWLEDGEMENTS

Immense gratitude is due to a great number of wonderful people. First and foremost I would like to thank my family for supporting me, for commiserating with me, and keeping my spirits up when things looked dark. Assistant Professor Paul H. Miller, of the Naval Architecture and Ocean Engineering Department at the Naval Academy and my research advisor, pushed me farther than I thought I could go, and was always ready with a smile and a helping hand. Extra thanks are due to Mr. John Zselecsky and Mr. Bill Beaver of the Naval Academy who somehow managed to save my project when all looked lost. Additional thanks are due to Mr. Gary Gibson of the Naval Academy, and Mr. Bill Day and the late Mr. Bruce Crook of the David Taylor Research Center. Special thanks are due to Mr. Joe Laiosa of NAS Patuxent River for his wonderful help with SPLASH, and to Mr. Paul Bogataj for his assistance with X-Foil and PANAIR. I cannot forget my roommate Pat O'Brien who listened to me complain and then told me how much harder his life was, but was always there. Thanks to my classmates in the naval architecture major at the Naval Academy who endured the struggle with me. Last, but not least, I must express my appreciation for Professor Joyce Shade who works so hard every year to make this program a success.

TABLE OF CONTENTS

ABSTRACT.....	1
ACKNOWLEDGEMENTS.....	2
TABLE OF CONTENTS.....	3
LIST OF TABLES AND FIGURES.....	4
THEORY.....	5
EXPERIMENTAL OVERVIEW.....	10
ANALYSIS OVERVIEW.....	14
EXPERIMENTAL WORK AND DATA ANALYSIS: INTRODUCTION.....	16
MODEL TESTING.....	17
THEORETICAL DEVELOPMENT ANALYSIS: FINITE ELEMENT ANALYSIS.....	30
THEORETICAL DEVELOPMENT: COMPUTATIONAL FLUID DYNAMICS.....	29
DATA REDUCTION AND CORRELATION.....	31
TANK TESTING: EXPERIMENTAL PROCEDURE.....	36
TANK TESTING: DATA ANALYSIS METHOD.....	52
TANK TESTING: DATA ANALYSIS RESULTS.....	58
DATA ANALYSIS: FINITE ELEMENT ANALYSIS RESULTS	61
CONCLUSION.....	69
RECOMMENDATIONS FOR FURTHER STUDY	69
ENDNOTES.....	71
BIBLIOGRAPHY.....	72

LIST OF FIGURES

Figure 1: Forces Acting on Wing Sections.....	6
Figure 2: Naval Academy 380-ft towing tank.....	11
Figure 3: Sampling Rate Diagram.....	12
Figure 4: Finite Element Displaced View of High Aspect Ratio Rudder.....	14
Figure 5: Span wise Pressure Distribution for Model Rudder.....	13
Figure 6: Strain Gage Locations.....	22
Figure 7: Experimental Setup Illustration.....	26
Figure 8: Dataforth Signal Conditioner and Data Acquisition Setup.....	29
Figure 9: Chordwise Pressure Distribution on Surface of Rudders.....	32
Figure 10: Spanwise Pressure Distribution on Surface of Rudders.....	33
Figure 11: CFD Correlation Diagram.....	35
Figure 12: Flow Pattern During Fully Dynamic Test Case.....	41
Figure 13: Model in Dynamic Test.....	43
Figure 14: Model Preparation.....	44
Figure 15: Rudder Swap.....	45
Figure 16: Flow Pattern Around Rudder—Slow Speed Test.....	46
Figure 17: Rudder Swap/Equipment Layout.....	47
Figure 18: Mr. John Zselecsky, Motor Layout, and Yaw Arm/Clamp.....	48
Figure 19: David Taylor Model Basin—Carriage 3.....	48
Figure 20: Towing Point, Yaw Arm, Roll, Pitch, and Yaw Pivots.....	49
Figure 21: Towing Point, Yaw Arm, Roll Springs.....	49
Figure 22: Motor and Stop Mechanism and Rudder Gage Board.....	50
Figure 23: Yaw String.....	50
Figure 24: Carriage 3—David Taylor Model Basin.....	51
Figure 25: Mr. Bill Beaver Operating Motor Circuit.....	51
Figure 26: Sample Strain Plot for Shaft Gage.....	52
Figure 27: Sample Side Force Plot.....	53
Figure 28: Sample Rudder Angle Plot.....	53
Figure 29: Sample Yaw Moment Plot.....	54
Figure 30: Rudder Loading for Slow Speed.....	58
Figure 31: Rudder Loading for High Speed.....	59
Figure 32: High Aspect Ratio Strain Plot—High Speed.....	62
Figure 33: High Aspect Ratio Rudder Static Loading Curve.....	64
Figure 34: Low Aspect Ratio Rudder Static Loading Curve.....	64
Figure 35: High Aspect Ratio Rudder Shaft Strain Plot.....	67
Figure 36: Low Aspect Ratio Rudder Shaft Strain Plot.....	68
Figure 37: The End.....	71

LIST OF TABLES

Table 1: Experimental Measurements.....	20
Table 2: Model Basin Testing Matrix.....	42
Table 3: High Aspect Ratio Rudder Data.....	65
Table 4: Low Aspect Ratio Rudder Data.....	66

THEORY

Force coefficients are non-dimensional forms of experimental data that apply to geometrically similar objects regardless of size, velocity, and fluid properties. In the case of a generic wing section such as an aircraft wing, a hydrofoil, or a control surface as in the case of a rudder or submarine control surface, the coefficient of lift allows an engineer to estimate the loads the wing section will be forced to support. The fluid force is described in equation (1), where F_x is the force acting on the body, C_x is the force coefficient, ρ is the density of the fluid medium, U is the average fluid stream velocity, and A is the projected area of the wing section

$$F_x = \frac{1}{2} C_x \rho U^2 A \quad (1)$$

normal (perpendicular) to the lift vector. Two orthogonal fluid forces act on an immersed body. The force of drag occurs parallel to the direction of fluid flow over the body as a result of shear stress acting between the viscous fluid and the surface and pressure drag. The force of lift occurs perpendicular to the drag force vector and the direction of fluid flow over the body. In the case of a control surface such as a rudder, the lift force produces the yaw moment that rotates the vessel in the desired direction.

The coefficient of lift, C_L , is determined experimentally using equation (1), where C_x is replaced by C_L . U , ρ , and F_L the force of lift, are measured experimentally, and A is known from the geometric configuration of the rudder. For each trial run the lift force is measured. After a series of data points have been collected, the average value for the coefficient of lift can be determined as a function of the angle of attack of the wing section into the fluid flow.

Steering a vessel involves the creation of an intentional misalignment of the lift forces acting below the waterline of a vessel in order to produce a moment to rotate the bow and the stern relative to one another.¹ For a transversely symmetrical body such as a ship's hull powered

directly from astern, no resultant lift (transverse) forces are generated as the section heads into the direction of fluid flow. However, as the body is inclined to the direction of flow pressure differences form on opposing sides of the body resulting in the generation of lift forces. Lift is produced by differences in pressure between different sides of a section.² As the flow meets the foil, it separates and proceeds around both sides of the section. For a symmetrical section inclined to the flow or an unsymmetrical section at zero angle of attack, the flow over the top and bottom of the foil proceeds at different velocities. As the flow increases velocity over one side compared to the other, the static pressure drops on that side of the body creating the pressure differential that produces lift. The Bernoulli equation shown in equation (2) applies in the case

$$P_1 + \frac{1}{2} \rho V_1^2 = P_2 + \frac{1}{2} \rho V_2^2 + losses \quad (2)$$

of nonexistent or negligible elevation change where P is the static pressure, ρ is the density of the fluid medium, and V is the fluid velocity relative to the body. 1 and 2 represent two generic points in the fluid stream. As velocity increases on a particular side, in order to maintain the energy balance the static pressure must drop. If the hull of the vessel is angled relative to this flow such as a vessel with a yaw angle due to the effect of wind or current, the hull itself will develop lift. This constitutes one of the components of lift below the waterline.

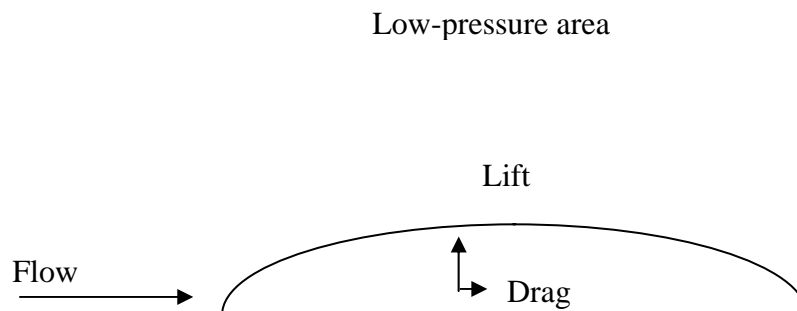


Figure 1: Forces Acting on Wing Sections

Rudder lift/drag efficiency for a given angle of attack is strongly influenced by the aspect ratio which has as one definition, the depth or span of the rudder divided by the average chord length as shown in equation (3). Larger aspect ratios with the same area result in more efficient

$$AR = \frac{T}{C} \quad (3)$$

rudders and generate a given amount of lift at lower angles of attack than rudders with lower aspect ratios, but also have a tendency to stall at lower angles of attack.³ Stall occurs after the rudder has reached its maximum coefficient of lift as the flow in the boundary layer separates from the rudder. The peak of the lift curve is precisely the goal of this project and experience has shown the transient dynamic peak may exceed the static peak. Determining this peak presents experimental difficulties resulting from the effects of free surface, ventilation, dynamics and stall. For example, as a vessel heels, or when in waves, the rudder approaches the free surface resulting in a phenomenon called ventilation. Ventilation occurs if the rudder is close enough to the surface of the water that the waterline on the low pressure side drops far enough that air replaces water next to the blade of the rudder resulting in a significant loss of lift.⁴ The ventilation effect will also change the expected values of the lift coefficient and maximum lift for that angle of attack.

The need for more efficient rudders with higher aspect ratios led to greater bending moments in the rudder shaft. As a result the majority of the loading on the rudder shaft is generated by this bending moment initiated by the lift force rather than the torsion resulting from the rudder's desire to return to its equilibrium position. At the same time rudder shaft diameters have become smaller as the higher aspect ratios require shorter chords and section percent

thickness has stayed around 12% of rudder chord. The combination of smaller diameter shafts and larger bending moments has caused significantly higher bending stresses.

The bending stresses present in the rudder shaft are determined by analysis of the strains measured in the shaft. The net pressure against the body of the rudder creates a force that is a function of both net pressure against the surface and the area of that surface as shown in

$$F = PA \quad (4)$$

equation (4) where F is the resultant force, P is the average pressure against the surface and A is the projected area of the surface. This force acts at the center of effort of the rudder surface. The distance from this point to the bearings where the shaft penetrates the hull produces the bending moment, which is equal to the force times the distance from the shaft bearing. The bending stress is then equal to the bending moment times the y, which is the distance from the neutral axis of the shaft to the outer fibers (i.e. the center of the shaft to the outer edge), times by the second moment of area (moment of inertia), I, of the shaft cross section as shown in equation (5)

$$\sigma = \frac{(Fd)y}{I} \quad (5)$$

where F is the hydrodynamic force from equation (4), d is the distance from center of effort to the lower shaft bearing and σ is the bending stress in the shaft. The strain is related to the stress by the modulus of elasticity, E, a material property. Strain is equal to modulus of elasticity times stress as shown in equation (6) where ε is strain, σ is the stress, and E is the modulus of

$$\varepsilon = \frac{\sigma}{E} \quad (6)$$

elasticity. The goal of this project is to reverse engineer these equations with the strain being the measured quantity in order to solve for the hydrodynamic force acting on the rudder surface so that it can be entered into equation (7), which is merely equation (1) solved for the dynamic lift

coefficient, C_L . F_L is the hydrodynamic lift force, ρ is the density, U is the relative stream velocity and A is the projected area of the rudder surface.

$$C_L = \frac{2F_L}{\rho U^2 A} \quad (7)$$

EXPERIMENTAL OVERVIEW

The experimental determination of C_L and the center of effort of the rudder are quite challenging and no published data exists for modern, high aspect ratio rudders. In order to record the data points for the coefficient of lift it is necessary to experimentally measure the forces and points of application of lift and drag on the rudder. To determine these quantities it is necessary to use strain gages and force blocks. Essentially strain gages are bonded to the structure under investigation so that the deformations of the structure and of the gage are equal. The sensors measure the voltage passing through the wire and this is calibrated through the application of known forces and zeroed. As force is applied to the body the wire is either stretched or compressed thereby changing the properties of electrical resistance. As the resistance increases or decreases the voltage changes proportionally. The calibrated voltages read as strain in the material. In this experiment the 1/2-inch gages were bonded to the surface of the rudder with epoxy, and utilized a quarter-bridge amplifier.

The experimentation was originally to include twenty-four runs in the 380-foot towing tank in the Naval Academy Hydromechanics Laboratory (Figure 2). However, due to Hurricane Isabel damage, data collection took place at the David Taylor Research Center in Carderock, Maryland. The basic tests had the model towed down the tank at normal speed and then the rudder was put “hard over” or pushed from the neutral position all the way against the mechanical rudder stops. Test variations included high speed in still water, waves, and with a heel angle, using a sixteen foot long, 1/5-scale model. The Naval Academy Model Shop in Rickover Hall between April and September, 2003 constructed two rudders and keel for the experiment. The model was loaned but the hardware, including the force blocks, instrumentation

and data acquisition system was developed with the strong support of the USNA Hydromechanics Lab and Structures Lab Group staff.

The model used an electric motor to change the angle of attack of the rudder and to return it to its equilibrium position. Using this device, a series of strain data points could be collected in each of the trial runs. Data were collected through the use of strain gages attached to the rudder shaft, with a reference gage attached to the hull to determine changes in the readings due to tank water and other environmental conditions. These gages fed data to a laptop computer mounted in the towing carriage. An adjustable voltage supply mounted in the vessel served as a portable power source for the gages.

The towing setup illustrated in Figure 2 shows the towing carriage attached by vertical



Figure 2: Naval Academy 380-ft towing tank

shafts to a model vessel. This is a similar set up to the David Taylor system. The model can possess up to five degrees of freedom; surge, heave, roll, pitch and yaw. Roll, pitch and yaw can also be fixed depending on the nature of the specific experiment. In the carriage were force blocks, box-like metal structures that deformed as load was applied producing voltage readings

similar in concept to the strain gages. For this experiment the force blocks measured side force and resistance, in addition to the strain gages mounted on the rudder shaft

The setup for the rudder shaft itself involved the placement of approximately eight strain gages on the shaft itself, three each aligned with the direction of bending and one on the other side of the shaft to measure the load perpendicular to the bending, i.e. the drag loads. The three strain gages on the sides experiencing the bending were placed at several different angles in order to provide the information to solve for the strains. The gages were calibrated and zeroed for a no load baseline condition. Data acquisition passed through 16 channels, with each channel capable of acquiring data for ten strain gages.

The sampling rate for the gages was a crucial issue for the acquisition of the transient peak in waves and while the rudder is turning. The difficulty was to have enough data points so that the peak value did not fall too far between successive data points. Otherwise the maximum forces derived from the data could have been lower than actual values. Initial runs indicated a sampling rate of 300 Hz for ten seconds would provide sufficient accuracy. Figure 3 illustrates the performance of different sampling rates in accurately describing a curve.

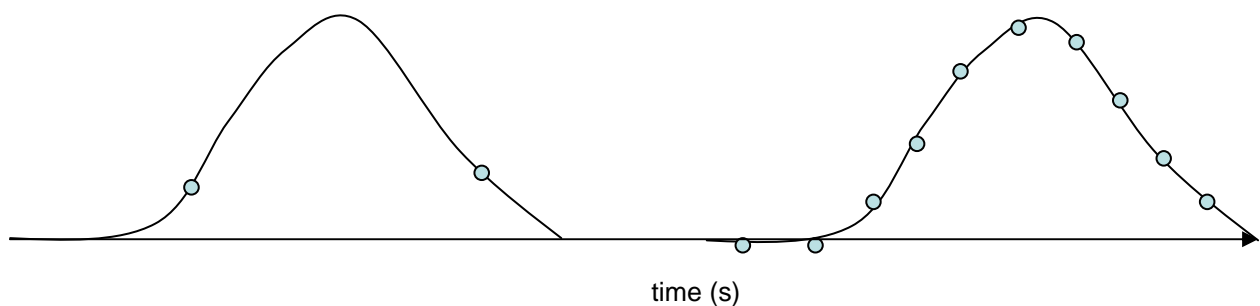


Figure 3: Sampling Rate Diagram

Another experimental setup difficulty arose from the sensitivity of the strain gages and the data collection systems. A sufficient strain to excite the strain gages on the rudder shaft had to occur for these instruments to pick up useable values. This is a major determining factor in the necessary model size. The shaft had to be stiff enough so that errors were not introduced into the data and sufficiently flexible so that recognizable values could be obtained. The three quarter inch aluminum shaft was an adequate choice.

ANALYSIS OVERVIEW

The peak rudder shaft strains were used to determine the corresponding rudder lift force. The primary tool for this process was a finite element analysis (FEA) model of the rudder and shaft. These models were constructed using a software package, COSMOS/M, which is a PC-based code installed on one of the midshipmen research computers in the NAOE Department. Figure 4 shows a finite element model of the high aspect ratio control surface. The model includes all the material properties and geometry of the actual rudder. The assumed pressure distribution was predicted using PANAIR, a fully submerged computational fluid dynamics (CFD) code run by Paul Bogataj. The chordwise pressure distribution was predicted using X-

Line STRAIN Lc=1

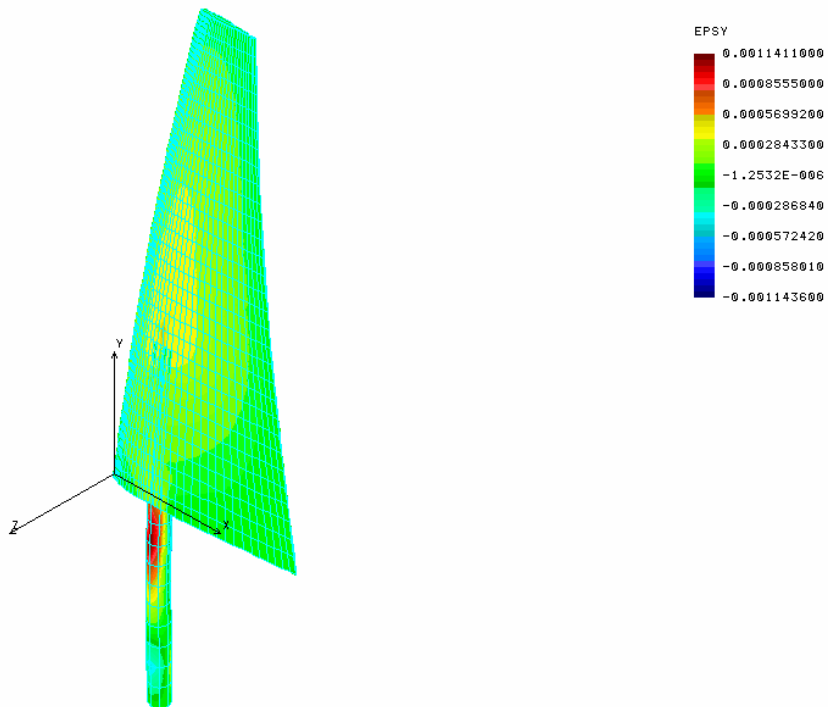


Figure 4: Finite Element Displaced View of High Aspect Ratio Rudder

Foil, a 2-D viscous code. With the known pressure distributions, which can be scaled for different velocities, the predicted strains were adjusted to match the measured strains. Figure 5 shows the initial assumed spanwise pressure distribution.

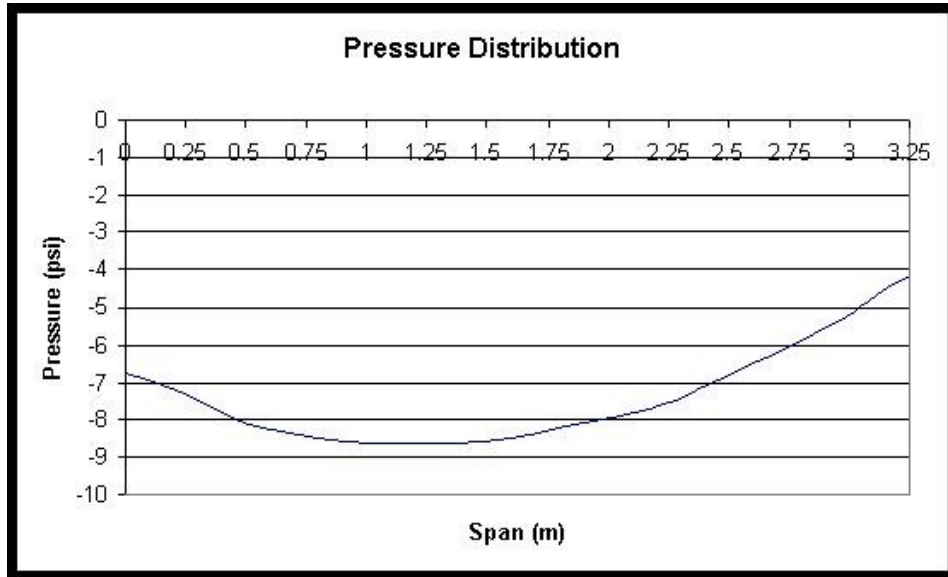


Figure 5: Spanwise Pressure Distribution for Model Rudder

EXPERIMENTAL WORK AND DATA ANALYSIS: INTRODUCTION

This investigation consisted of three parts. With the support of the Naval Surface Warfare Center (NSWC), the primary part, the model-testing was moved to the David Taylor Model Basin at Carderock, Maryland. The second part of this project was the correlation of the experimental material strains obtained by the various measurements collected during the model testing portion of the project with the forces necessary to cause such deformations through the use of a finite element model. The finite element model was constructed based on the physical composition of both rudders and their attached shafts. The finite element model used an interconnected polygonal mesh and solved for the forces acting over the surface of the rudder and shaft. The inputted strain data read from the experimental analysis was solved in the program using matrix methods. The third part of this analysis consisted of using a computational fluid dynamics software package in order to correlate the experimentally derived forces along the foil's surface to the accompanying flow patterns. These parts of the project were merged into the final data analysis and results. Each aspect of the project mentioned briefly above is developed more thoroughly in the following sections.

MODEL TESTING

Generally tank testing is used to predict the value of the drag, or in naval architecture terms resistance, caused by a fluid against the ship's hull. As a ship moves through a fluid medium such as water, it experiences a resistance as a function of its velocity through the fluid. William Froude was the first to determine that fluid resistance on the air—water interface is composed of two effectively separable components of resistance, i.e. frictional resistance due to the interaction of water and the skin of the ship and residual resistance due to the energy required to produce waves. Frictional resistance is further subdivided into two orthogonal components of tangential or skin friction caused by wall shear stress and normal or pressure drag caused by the distribution of pressure forces on the body. The skin friction is a result of fluid passing along the surface of the hull in a direction opposite to the motion of the ship relative to the fluid. In resistance calculations skin friction is defined by the Coefficient of Skin Friction (C_f). The normal component of friction is a function of the geometric hull shape of the ship which is represented by the constant K , the Form Factor.

As the ship passes through a fluid along the air—water interface, gravity waves result from pressure differences along the sides of the ship's hull. Wave making resistance constitutes the primary source of residual resistance due to the ship's passage through water. Energy from the ship's propulsion source forms the wave and therefore detracts from the energy directed in pushing the ship forward through the water. A similar pattern of divergent and transverse waves is created for model and ship. Frictional resistance is a function of velocity of the ship through the water V , length of the ship L , and viscosity of the water ν . Functions using the non-dimensional quantities of Reynolds number, equation (9), and Froude number, equation (8) are used to approximate the frictional and wave-making resistances of ships, respectively. As can

$$F_N = v / (gL)^{1/2} \quad (8)$$

$$R_N = \rho v L / \mu \text{ or } R_N = V_s L / v \quad (9)$$

be ascertained from the relationships for resistance, scaling both types of resistance from a model to geometrically similar ship cannot be accomplished using a single scaling factor. Froude broke the two components of resistance apart and scaled those using separate scaling factors and added the components back together at the end. Thus scale model testing in model basins became an effective method of calculating resistance for larger vessels. Total resistance of a vessel in a model basin can be calculated through the means of a towing carriage and a force block.

In this experiment, the resistance of the fluid against the vessel was ignored, and instead the problem that was analyzed was the effect of this fluid flow as it interacts with the ship's hull and control surfaces at the free surface. What makes this problem so interesting is that effects such as ventilation and wave generation at the free surface make the simplified equations used in classical wing theory invalid for these complex problems.

Due to the complex nature of the fluid-structure interaction problem, an accurate and reliable mathematical or computer model for the computation of the expected forces experienced in transient foil response has not been developed. Although reliable computational fluid dynamics models have been developed to handle the forces as experienced in powering, static turns, and foil analysis, computer models cannot predict with a significant degree of accuracy what the response of the fluid/foil interaction would be given a set of operational conditions. Real world effects such as free surface effects created where the foil, in this case the rudder, either pierces or is significantly near the free surface where the interface between air and water occurs such that effects like ventilation and wave-making occur. As the pressures on opposite sides of the rudder blades diverge greatly, air is sucked into a cavity near the rudder. Modern

fluids software packages cannot account for this. In addition, classical wing theory as described above provides lift coefficients for static foil analysis. In this case, as the rudder is inclined to the flow, it experiences a force spike before settling down to the static lift value. These and other aspects of transient foil analysis were explored through the model testing.

The experimental measurements are described in Table 1. The number of experimental values presented one of the greatest challenges to the success of the model testing portion of the experiment. Furthermore, the high data sampling rate required to adequately define the time history of each of these experimental values presented another source for potential problems. The Hewlett Packard 3852 Integrating Voltmeter with a multiplexer collected the data on up to twenty-four different data collection channels. The computer program governing the operation of the integrating voltmeter and the multiplexer allowed sufficient control over the data sampling rate for each data channel. For example, the strain gages measuring the deformation in the rudder and shaft material were run at a sampling rate approaching 300 Hz while less important values such as the vessel motions and redundant gages were run at a slower rate to allow for higher speed on the more critical values.

Measurement	Priority/Channel	Device
Vertical Shaft Gage	1	Rosette (1)
Vertical Shaft Gage	2	Rosette (2)
Velocity	3	Tachometer (DT)
Rosette Gage	4	Rosette (1)
Rosette Gage	5	Rosette (1)
6" Rudder Gage	6	Strain Gage (1)
12" Rudder Gage	7	Strain Gage (2)
Side Force	8	Towing Point Force Block
Yaw	9	Force Block
Pitch	10	Potentiometer/Pulleys
Heave	11	Stringpot
Roll	12	Potentiometer/Pulleys
Rudder Angle	13	Potentiometer
Wave Height	14	Wave Probe
Rosette Gage	15	Rosette (2)
Rosette Gage	16	Rosette (2)
6" Rudder Gage	17	Strain Gage (3)
12" Rudder Gage	18	Strain Gage (4)

Table 1: Experimental Measurements

What follows is a basic description of the experimental method that was used to measure the values shown in Table 1 above. The deformation of the rudder shaft and rudder blade materials were measured by the use of 8 350-ohm strain gages and 350-ohm rosettes consisting of three strain gages stacked on top of one another at forty-five degree angles.

A strain gage operates on the basic principles of Ohm's Law shown below in equation (10) where V is voltage, I is electrical current, and R is resistance. The gages were bonded firmly to the surface of the material to be measured so that as the surface deforms, the gages deformed at exactly the same rate. As the gage stretches or contracts

$$V = IR \quad (10)$$

along with the material of interest, the length of the wiring inside the gage increases thereby increasing the gage's resistance. As a result, the corresponding voltage output from the strain gages varies linearly with the resistance. Assuming two points of applied deformation and the corresponding force are known, the calibrated voltage output can be read as strain or deformation in the material. For small deformations such as these, the deformation is linear. The general method that is used for strain gage calibration is to zero the voltage reference when no loads are applied to the structure and then to apply different known loads and measure the voltage output. These data points allow for the voltage output to be transformed and read directly as strain.

The specific location of the strain gages described in Figure 6 permitted the collection of strain data at several key locations along the rudder surface. Channels 1 and 2 measured the bending moment in the rudder shaft due to the hydrodynamic effects on the surface of the foil. Since the hydrodynamic forces acting on the surface of the foil can be resolved into a single force acting at the center of effort of the foil, the magnitude of the bending moment created by the expected hydrodynamic forces was estimated using beam theory. For the more detailed post-experimental analysis the finite element model correlated the expected pressure distribution across the rudder developed from the computational fluid dynamics model with the experimental strains measured

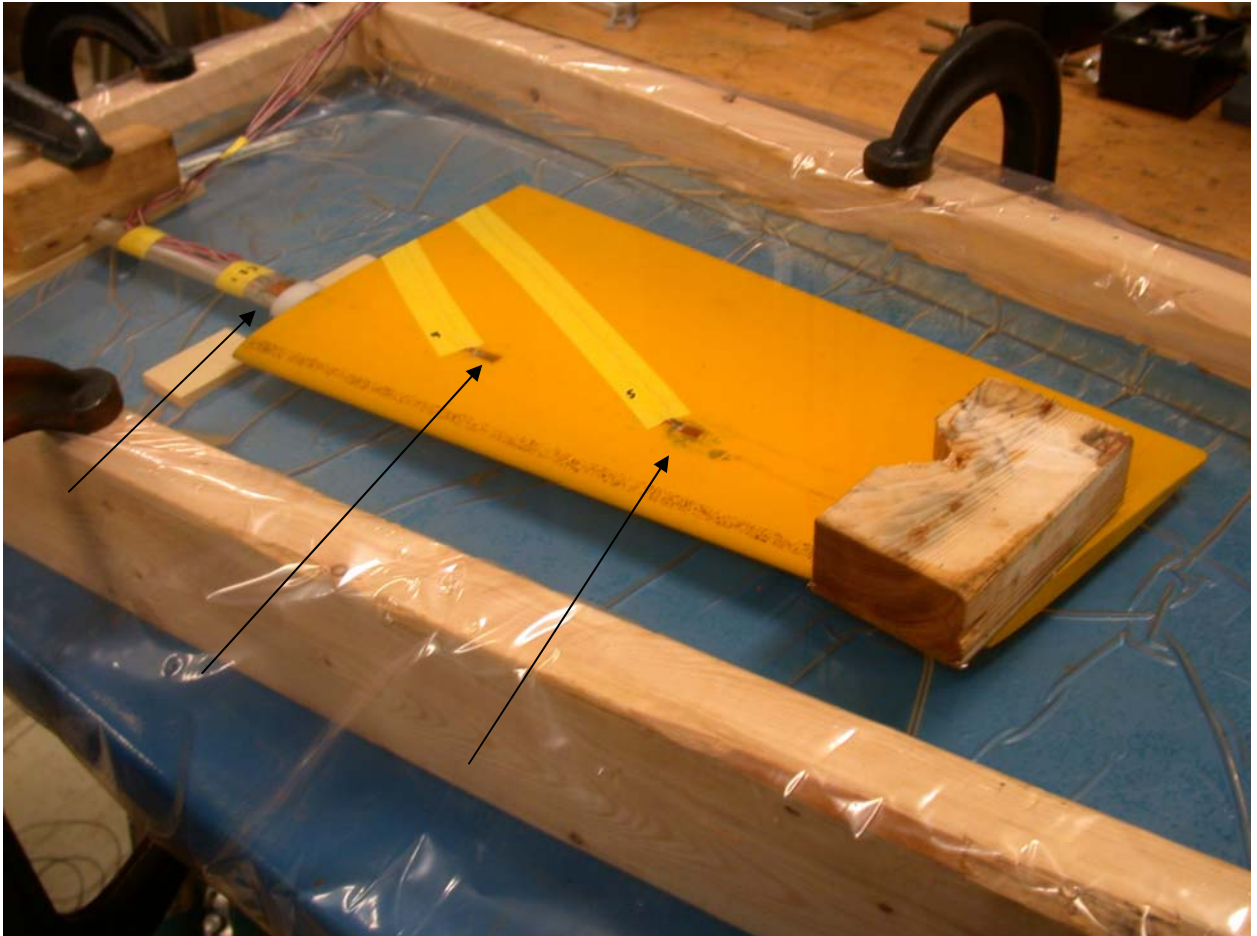


Figure 6: Strain Gage Locations

from the values just described. As shown in Figure 6 and Table 1, the gages measuring the strain along the axis of the shaft were part of the forty-five degree rosettes mounted on either side of the rudder shaft.

Also contained in the rosette are four gages, two on either side of the shaft, at forty-five degree angles from the main axis of the shaft. These gages measure the strain due to the torsion of the shaft under the hydrodynamic effects of the fluid and foil. Ideally, the shaft should not have to resist large torsional loads due to the placement of the rudder shaft along the quarter chord length of the rudder. This is the point on the rudder one quarter of the chord distance from the leading edge of the foil, where

according to classical wing theory the hydrodynamic center lies. This means that since the resultant hydrodynamic force is in line with the rudder shaft no torsion is developed. The collection of these values allows axial deformation of the shaft due to torsion to be calculated so that it does not bias the final results. Four additional single gages located at points six and twelve inches from the root of the foil measured the deformation of the rudder blade due to hydrodynamic action allowing for additional calculation and verification of the bending moment. Due to the non-isotropic nature of the composite rudder blade, simple beam theory could not predict an accurate value for the bending moment, but it provided a reasonable order of magnitude check on the finite element output that was developed later in the analysis. In the correlation developed in the more accurate finite element model, these strains derived from tank testing were correlated to the forces and the pressures experienced across the surface of the blade in the same manner as the gages on the shaft. The two additional strain gages, again located on opposing sides of the rudder and shown as channels 19 and 20 in Table 1 acted as reference gages allowing for any deformation in the gages due to environmental effects such as temperature to be removed so that bias was eliminated from the final analysis.

In order to determine the actual, experimentally determined vertical center of effort of the foil and by extension the actual resultant force of lift developed by the foil, it is necessary to combine a measurement of the yawing moment developed by the rudder with the bending moment induced in the rudder shaft. Based on the equations of static equilibrium, developing a system of two equations allows the variables for the center of effort and force of lift to be calculated. A finite element model will correlate the

experimental values with the pressure distributions necessary to create this resultant force and the values for strain collected from the gages.

To develop the second equation, two values of force were measured. By measuring two values of force and again utilizing the equilibrium equations, the yawing moment of the vessel due to the action of the rudder was calculated. The experimental setup developed to calculate these values is as follows. To measure the value of side force acting on the body of the model, a 4-inch force block was attached directly below the attachment point of the towing carriage heave post. The force block acts as a spring in the same manner as a strain gage. The arms of the force block are fabricated to a specified thickness so that load within a certain range for which the gage is designed will cause plastic deformation (i.e. non-permanent change in the shape) of the force block from a cubic or rectangular shape to a polygonal shape. As the force block stretches under the load, the calibrated voltage drop across the gage is read as the force applied to the gage. These gages are calibrated in a similar manner to strain gages. Since these force blocks also follow Hooke's Law, equation (11), the deformation and voltage changes are linear where σ represents stress, E the modulus of elasticity, and ϵ the strain

$$\sigma = E\epsilon \quad (11)$$

or normalized deformation. Again using Ohm's Law, the resistance of the force block increases, or decreases under load, changing the voltage output. In order to determine the yawing moment about the towing point, a second value of force is required. This second value of force came from a two-inch force block attached to a U-shaped channel cantilevered above the roll and yaw pivots of the model. A second arm was cantilevered from the towing post above the level of the yaw bearing. A link and an adjustable

damper that provided stiffness and control in yaw connect these two arms. In this linkage system the force block was included so that the only load path from one arm to the other passed through this force block. Initially the lower arm rested against a rigid mechanical stop. As the vessel yawed due to the action of the rudder, the two arms, initially aligned, moved to separate as they rotated independently about the yaw pivot. As they separated, the force needed to yaw the vessel passed through the damper and the force gage. Since the distance between the measurement point and the towing post was known to be three feet, the moment causing the boat to yaw was determined. The force causing the vessel to yaw was provided by the action of the rudder, and since the horizontal distance from the center of yaw to the center of effort of the rudder along its quarter chord length is known, the force of lift required to yaw the vessel was calculated. The experimental setup described in the preceding paragraph is illustrated in Figure 7 and described in Figures 17-25.

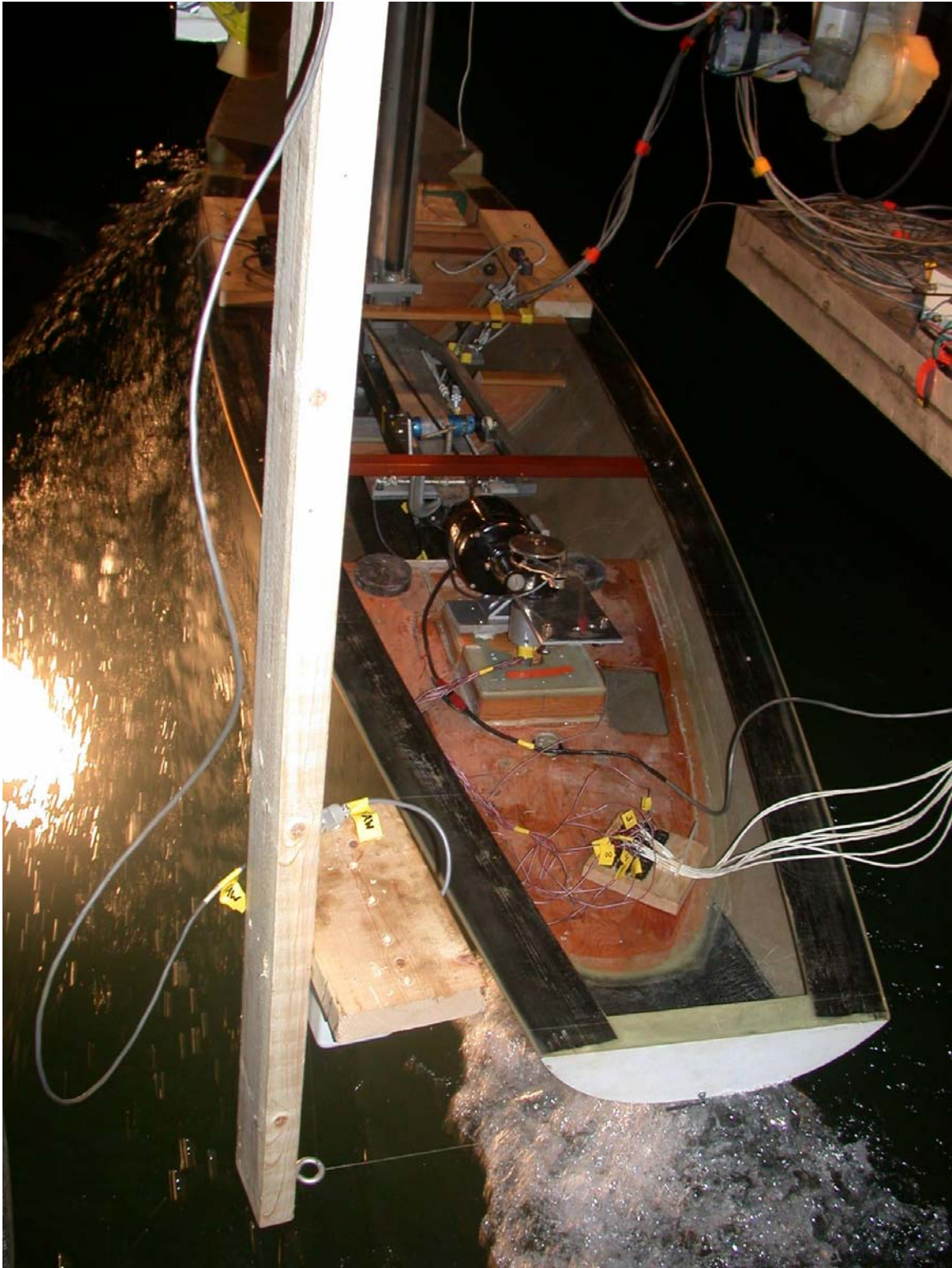


Figure 7: Experimental Setup Illustration

In addition to the experimental values already explored, the final analysis required a correlation between the motions of the vessel and the forces developed by the vessel and its rudder. Experimentally, these motions were determined through the use of potentiometers or variable resistors, and stringpots. To measure the motions of pitch and roll, two circular potentiometers were attached by a gear/pulley system directly to the shafts that facilitate the movement of the model. As the model rotates about the shaft, the gear attached to the potentiometer turns proportionally with respect to the gear ratios with the output read as a calibrated voltage output. The angle of attack of the rudder relative to the longitudinal axis of the hull was also measured with a potentiometer. A stringpot acts on a similar principle, except that it is designed to measure linear instead of rotational displacements. A string extending from the mechanism is attached to a point of interest, and as that point moves a variable resistor inside of the stringpot is adjusted proportionally. The stringpots in this experiment were used to measure the heave or vertical rise of the vessel, and the deflection of the stern due to yaw.

Each element of the data collection puzzle required a calibration within the range of expected output parameters. For example, the main force block gage values were expected in the range from 0-200 pounds. Successive voltage measurements were made on the force block output as increasingly higher loads are placed on the body. As the load increased, the resistance of the gage changed producing a proportionally equivalent voltage output. For each incremental change in the measurement parameter, the output voltage was collected and then plotted against the measurement parameter. All of the gages used in this experiment remained within the linear elastic range of deformation and deflection; therefore the slopes of these curves were approximately linear. For each of

the data channels sampled in this experiment, the standard deviation of the values was calculated in order to arrive at a measure of the precision of the gage. Mr. John Zselecsky and Mr. Bill Beaver of the Naval Academy Hydromechanics Laboratory performed much assistance, planning, and construction for the setup, assembly and calibration of these data acquisition channels, and the necessary mechanical hardware.

The data collection itself was accomplished with the help of the TSD Structures Division. A Hewlett Packard 3852A Data Acquisition Center was used in conjunction with a multiplexer to sample over the range of channels and then feed these outputs onto the hard drive of a personal computer. The HP 3852 utilizes multiple modules depending on the requirements of the experimenter. For the purposes of this experimentation, a multiplexer with sixteen channels was used to monitor eight transducers and eight strain gages located on the rudder shaft and blade. The data acquisition center was given its commands through a program called VEE by Mr. Gary Gibson of the TSD Structures Division. For the strain gages a Dataforth signal conditioner was used to amplify the signals given by the gages under strain. Each of the gages required a quarter bridge rectifier module and five volts of excitation (power) in order to provide a usable signal. The gages themselves were Vishay Micro-Measurements 350- Ω strain gages, selected to reduce noise from stray voltages, radio frequency signals, and to reduce the signal degradation caused by operating under water. Each data channel was sampled at an average rate of 300 samples per second. Each individual channel sampling rate was adjustable using the programming and commands to the HP 3852. The data acquisition

center was able to process 4096 samples per second. Each piece of data was then

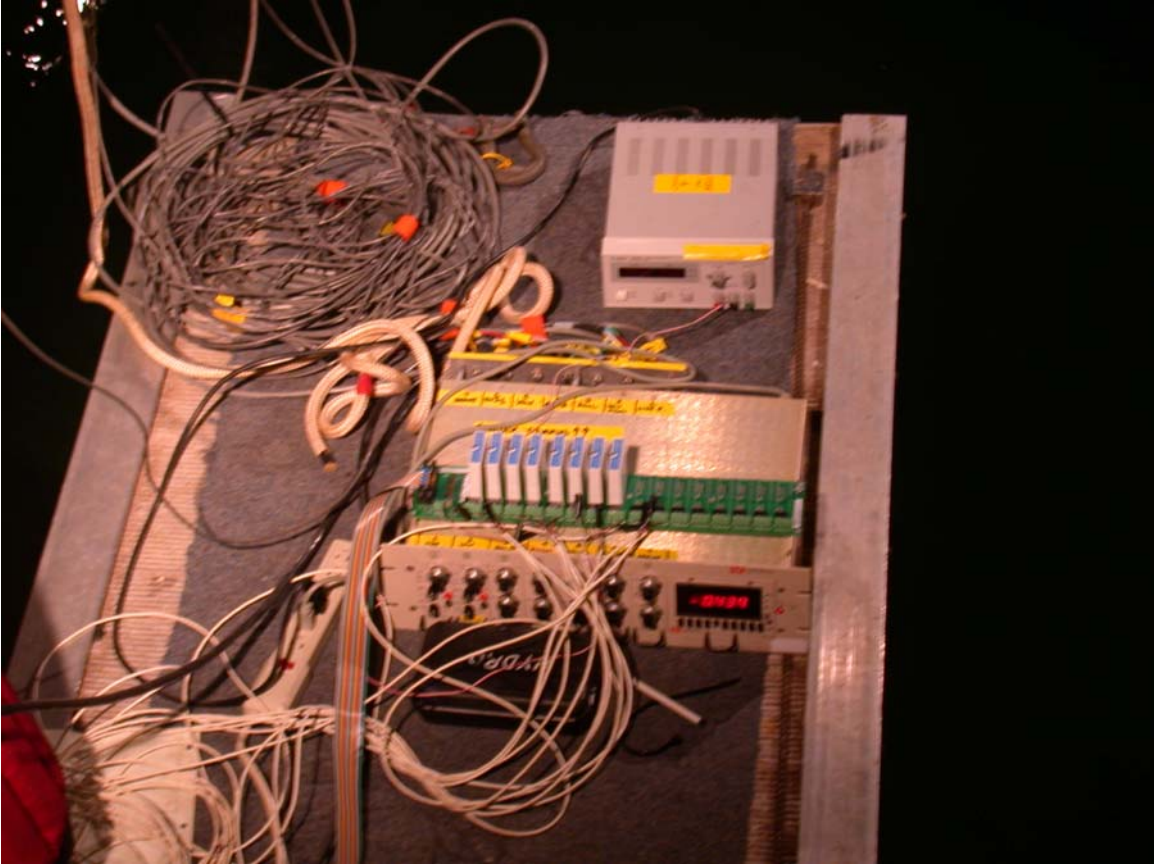


Figure 8: Dataforth Signal Conditioner and Data Acquisition Setup

transferred to the hard drive of a personal computer for later data analysis. Each of these experimental measurements provided a slice of the information needed in data analysis. Figure 8 shows the Dataforth quarter bridge rectifier set and accompanying data collection hardware mounted on a platform during the testing at the David Taylor Research Center.

THEORETICAL DEVELOPMENT: FINITE ELEMENT ANALYSIS

As mentioned in the theory section of this report, finite element analysis allows for the investigation of stresses and strains in complex composite structures using both linear and non-linear direct stiffness methods. The program used in this analysis was COSMOS/M software by Structural Research and Analysis Corporation. The program allows for the construction of multiple layers of surfaces bonded together and given different boundary conditions, material properties, loads, strains, pressures, and many other intrinsic and extrinsic properties of the structure. Once the real world structure is in its final form, the finite element model is developed to match the structural properties with a known set of forces. The program then calculates the expected stresses and strains in the structure. For the purposes of this experiment, material properties, structural configuration, expected pressure distribution, and expected pressures were inputted into the finite element program in order to solve for the strain on the rudder surface and ultimately its non-dimensional form as the dynamic lift coefficient.

DATA REDUCTION AND CORRELATION

This section deals with how this project was drawn together to evaluate the method of using computer analysis tools to predict the lift forces for a control surface operating at the free surface of a fluid body. X-Foil, a two-dimensional fluid dynamics code that gives the Reynolds number dependent coefficient of lift for the foil was used. The X-Foil analysis is a viscid code meaning that it takes into account friction and the effects of flow separation, thereby providing a theoretical peak for the curve of the coefficient of lift plotted against the angle of attack. To validate this analysis one specific condition derived from the experimental data was chosen. This condition provided for freedom for the vessel in yaw, however no freedom in the roll motions. The vessel, in addition, was in the upright condition. This condition was chosen because it eliminated many of the variables in the test matrix allowing for analysis in conditions that are within the range of capabilities of the computational fluid dynamics programs. To most accurately represent the conditions near stall, the spanwise and chordwise distributions were calculated at an angle of attack of 15 degrees.

Once the computer codes were run, the approximated coefficients of lift along the span of the rudder from the root to the tip were inserted into a spreadsheet and integrated along the span of the control surface to develop the lift force profile. This used the lifting-line theory applicable to high-aspect ratio lifting surfaces, such as the rudder, for each of the angles of attack developed in the tank testing. These ranged from zero to five degrees of yaw angle, and from zero to thirty degrees of rudder angle. This developed a computer-based model of the lift curve, the expected maximum value of the coefficient of lift as a function of the angle of attack, and the pressure given as a function of the

distance along the span of the foil. Figure 9 shows the chordwise pressure distribution for each rudder. Figure 10 illustrates the spanwise pressure distribution developed from PANAIR, a 3-D inviscid CFD code.

The pressures developed in the above paragraph were then inserted as the load along the control surface in the finite element model of the rudder to approximate the values of the strains measured at every point on the foil surface. The validation of this method of computer analysis involves comparing these computer-derived values for the strain at the location of the strain gages, to the actual values measured from the strain gages in the tank testing experiments. The data reduction procedure is illustrated in Figure 11.

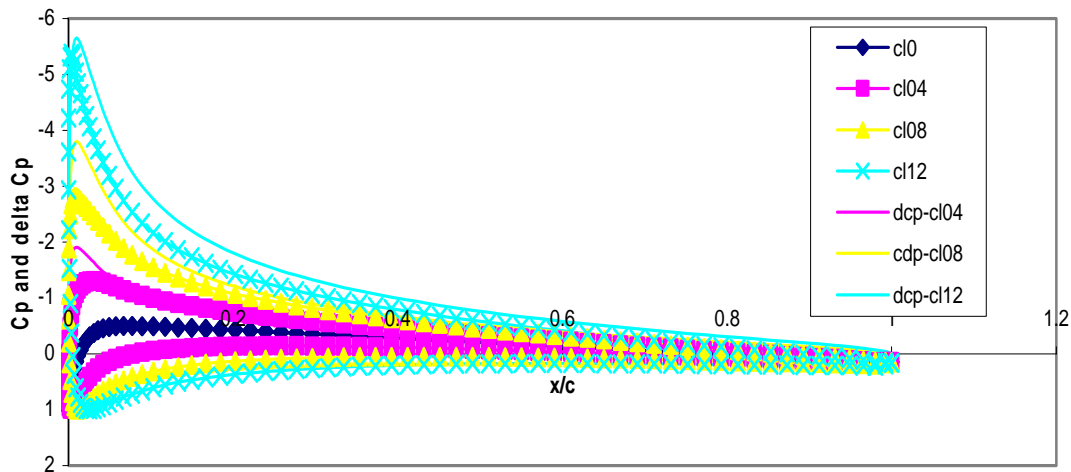


Figure 9: Chordwise Pressure Distribution on Surface of Rudders

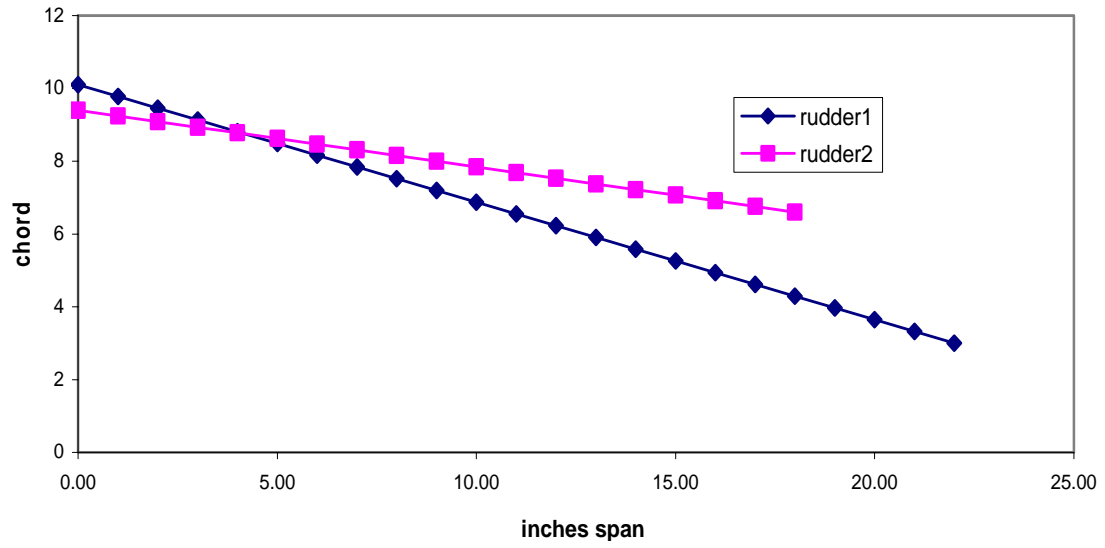


Figure 10: Spanwise Pressure Distribution on Surface of Rudders

PANAIR
-three-dimensional
-inviscid therefore high coefficient of lift
-spanwise distribution

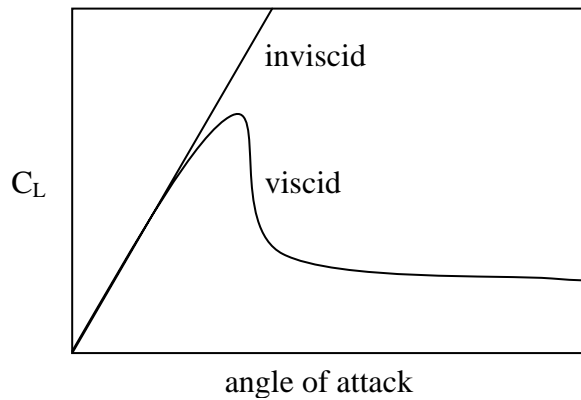
X-FOIL
-two-dimensional
-viscous analysis i.e. Reynolds Number dependent, chordwise distribution

↓

STRIP THEORY
-use simple lifting line rudder model

↓

MODEL OF LIFT CURVE
-degraded maximum lift coefficient



angle of attack

↓

SPANWISE LIFT (PRESSURE)



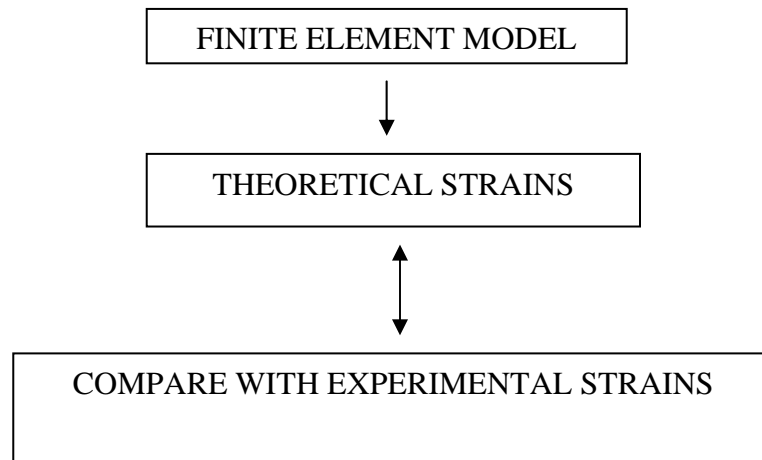


Figure 11: CFD Correlation Diagram

TANK TESTING: EXPERIMENTAL PROCEEDURE

The main point of this project was the experimental analysis of how lifting surfaces behave at the free surface of a real fluid medium under a number of different experimental variables. The technical description of the hardware used in the tank testing has been presented in an earlier portion of this report. What are described here are the different variables and experimental conditions that were explored in model basin testing and the experimental data collection runs that were designed in order to collect them.

An initial series of tests was conducted to calibrate and align the model sensors and mechanical gear. These runs were designed to determine the real axis of the model in the longitudinal direction. Starting at an assumed yaw angle of five degrees, the model was run down the tank and yawed through the entire range from five to negative five degrees with the keel attached but without a rudder or other lifting surface. This data was then analyzed in order to determine the actual angle for the zero side force and zero lift point. Once this point was calculated, it was marked as zero degrees yaw, and a mechanical restraining device was attached to the model in order to provide a rigid mechanical stop for the model and a convenient zero angle reference point for the electrical data collection systems. Once this calibration run was completed, several more zero angle calibration runs were made with the high and low aspect ratio rudders attached in order to develop an initial reference database of baseline zero degree yaw angle and zero rudder angle. This data was used to reference later dynamic runs and also supplied computational fluid dynamics data later on in the data analysis section. Once the baseline set of data was collected, a simple pitch and heave calibration was performed in order to

establish the sign conventions. Beyond this point the real data collection and experimentation began.

Three major and two minor independent variables were created, tested, and analyzed in the experimental testing and data collection. The first and most important were the series of variables that will be described as the dynamic model conditions or model degrees of freedom. These involved constraints of the model's ability to rotate around her yaw and roll axes, and the amount of damping applied to these motions in order to simulate actual vessel conditions. The second variable was the model speed. The model was towed down the tank at two different speeds in order to evaluate the change in dynamic lift coefficient with respect to speed. Every run that was performed was done first at the lower model speed followed immediately by the higher model speed. The third variable was aspect ratio. Most of the runs were performed with a smaller aspect ratio rudder modeling the types of vessel rudders used in common practice and nearly all of these runs were duplicated with a rudder mimicking a higher aspect ratio rudder currently seen in "high tech" maritime and sailing applications. The only data that was not collected for both aspect ratio rudders was the wave data due to the limited time allocated to wave data collection. The fourth variable tested was the rudder rotation rate. Two to three samples on every run were conducted at a constant value of rudder rate and then two different samples on every run were collected at two different higher rudder rates. The final variable that was tested was the change in loading due to the vessel's encounter with irregular waves as seen in an inshore sea-state spectrum. For each of these experimental model conditions, the data was collected, normalized, and analyzed in order to establish or disestablish data trends and correlation between the experimental

variables. For each of the variables that were altered, the resulting change in rudder loading was examined in order to determine which variables have the most effect on rudder loading and what percentage of increase or decrease in rudder loading can be expected as normalized by the baseline rudder data.

In order to analyze this trend most efficiently, the next series of runs was conducted for both the high aspect ratio rudder and the low aspect ratio rudder. The model was placed in the tank in an upright condition with zero degrees of yaw angle and was towed down the tank while the rudder was moved to different pre-selected locations in order to gather baseline rudder data and a quasi-static rudder loading curve. Starting at zero degree and moving in five degree increments until the rudder angle reached thirty degrees the rudder was moved to one of the prescribed locations, all transient effects were allowed to damp out, and then data collection was performed. This experiment was performed several times in order to establish the reliability of the data. This experiment established the basic lift curve up to stall that could be expected from a rudder operating in quasi-static conditions or a rudder on a vessel undergoing a steady turn with static rudder conditions once the vessel is indeed in its steady turn. The results for all experiments will be presented in the analysis and results section.

The boundary conditions of the model were altered to simulate the conditions that a full-scale ship experiences when executing a turning maneuver. The turn of a ship is divided into three recognizable phases. The first phase of a turn occurs immediately after the rudder of a ship has started to turn and ends when the ship develops a drift angle, i.e. an angle develops between the main axis of the ship and her direction of motion. This drift angle is referred to as β . Once the ship develops a drift angle she has entered the

second phase of her turn. The third phase of the turn occurs when the rate of change of the drift angle of the ship has fallen to zero, and the hydrodynamic forces along the ship's hull have balanced themselves out. The third phase of the turn is the steady state phase and results in a constant radius turn. While the rudder remains at constant deflection, the ship will remain in this constant rate of turn. The first and second phases of the turn, however, are transitory. The phase of interest in this analysis is the first phase of the turn. Once the rudder has reached its maximum angle of deflection, the first phase of the turn has ended and the ship has developed a drift angle. In this initial phase of the turn, the angle of attack of the rudder relative to the flow passing across the foil, and the angle of deflection relative to the longitudinal axis of the ship are in flux. It is during this phase that the forces on the rudder are changing most rapidly, and it is also the phase of the turn where the ship has not begun to dissipate the energy absorbed by the rudder by turning the ship. Hence the first phase of the turn sees the highest loading, and highest forces. In this analysis the model is not allowed to reach a full steady state turn due to the constraints of the testing apparatus, to be described later. However, the first phase and the beginning of the second phase of the turn were simulated in the model basin to resolve the peak loadings expected by the vessel.⁵ During this phase the dynamic conditions of the model were altered to reflect the dynamic conditions of the full scale vessel.

All of the remaining experimental data collection runs were done to establish the trends in rudder loading primarily as a function of the dynamic model conditions in order to compare these values to the results achieved for lift from classical wing theory. At this point, however, it is necessary to digress and explain the model dynamics as they were

altered and controlled during the course of this experiment in order to more clearly illustrate the selection of experimental conditions from this point. Pitch, heave, and translation were not fixed or damped except by the natural restraints imposed by the model and its accompanying mechanical apparatuses. Due to the linear nature of the model testing basin at the David Taylor Research Center, no translational motions were allowed in the direction of sway. The primary dynamic motions that were constrained were the roll and yaw of the vessel as these most readily affect the performance of a rudder when a vessel performs a maneuver. Under ideal conditions, the model would have achieved dynamic similitude in all degrees of freedom to the parent vessel, and no degrees of freedom would have been fixed. Such a test might have been performed by a self-propelled model in a seakeeping basin or larger body of water. However since these types of facilities were either unavailable or impractical, it was decided to use a normal linear model basin normally used for resistance studies and constrain the model in the following manner.

Roll motions were constrained in one of three manners. In the first analysis, the model was completely and rigidly fixed about its roll axis. In the second condition, the model was allowed to roll about its axis, but the motions were damped by springs in order to achieve a scaled roll period approaching that experienced by the parent vessel. In the third condition, the vessel was allowed to oscillate about its roll axis, however, the model was undamped, and was allowed to oscillate at the model's natural frequency, vice the scaled natural frequency of the parent vessel. The design of the motions for the yaw of the vessel allowed for experimentation of the effect of different yaw angles and yaw rates on rudder loading. In the design of the towing point for the vessel, a point was

picked that was nearest to the actual vessel's center of rotation so that the towing post of the vessel would not introduce an additional yaw moment and contaminate the analysis. A shock absorber was included in the model in order to allow the vessel to



Figure 12: Flow Pattern During Fully Dynamic Test Case

rotate at a frequency approaching the rate of rotation for a generic sailing vessel. Mechanical stops were attached to the vessel in order to allow it to rotate through an arc from five to zero degrees of yaw angle as though the vessel were sailing in the upwind condition and had to make a maneuver away from the wind as in bearing off. This maneuver requires the most force and hence rudder loading. Three different conditions for yaw were also designed and incorporated into the analysis. The first condition was designed for the model to be moving ahead at constant velocity at zero yaw angle with no

dynamic freedom in yaw. The second condition again did not allow for dynamic freedom in yaw but the model was rigidly fixed at a yaw angle of five degrees. The third condition was designed to allow the model to start against the stops at five degrees of yaw angle as though the vessel were sailing ahead but had some yaw angle in order to counteract the effect of wind. When the rudder was actuated, the vessel was allowed to rotate through the arc from five degrees to zero degrees of yaw from stop to stop. This condition is illustrated by the photograph in Figure 12. The only damping was provided by the hydrodynamic effects of the hull, rudder, and keel on the fluid and by the shock absorber placed in the model. In this experiment the amount of yaw damping was not varied. Each combination of these conditions in the matrix was conducted in order to determine the effects of each on rudder loading. The testing matrix used for both the high aspect ratio and low aspect ratio rudders is listed in Table 2.

Testing Matrix	
Case 1:	Fixed 5 Degrees Yaw/Free Roll
Case 2:	Fixed 5 Yaw/Fixed Roll
Case 3:	Fixed 5 Degrees Yaw/Fixed Roll
Case 4:	Fixed Zero Yaw/Fixed Roll
Case 5:	Free Yaw/Free Roll
Case 6:	Fixed Zero Yaw/Free Roll
Case 7:	Free Yaw/No Roll Damping
Case 8:	Low Aspect Ratio Rudder in Waves

Table 2: Model Basin Testing Matrix

For each point in the testing matrix, at least one experimental model run was performed to collect data. On each of these runs, as the model was towed down the towing tank at a constant rate, at least four data point were collected for each condition at each speed. Due to the fact that an electric motor with a control box for variable torque and variable speed was designed into the experimental system, the rudder could be sent

back and forth between the mechanical stops located at zero and thirty degrees of rudder angle multiple times during each data collection run. Given the five eighths of a mile length of the towing tank and the David Taylor Model Basin, this allowed for many data points to be collected during each towing tank run. As 15 minutes were required between successive runs to allow for the water to settle, minimizing the number of towing tank runs while maximizing the number of data collection cycles per run the testing matrix was as large as possible. It was especially important since each data collection cycle (i.e. each time the rudder was shifted from zero to thirty degrees) yielded only one data point. Each towing tank run took from fifteen to thirty minutes. This included



Figure 13: Model in Dynamic Test

accelerating the towing carriage to speed, collecting data, returning the carriage to the start, and allowing for wave damping. Each data collection cycle generally lasted less than five seconds. Eight experimental data collection cycles were able to be completed during each towing tank passage given the speed of the model and the length of towing tank available. To maximize utility, on each towing tank test, four samples were taken at the slower model speed. The model was then accelerated to the higher speed and the data taken. The time necessary for the carriage and model combination to accelerate to speed generally took less than one minute meaning that very little time was wasted in making this switch. Approximately two hundred data points were collected during the course of the experiment.

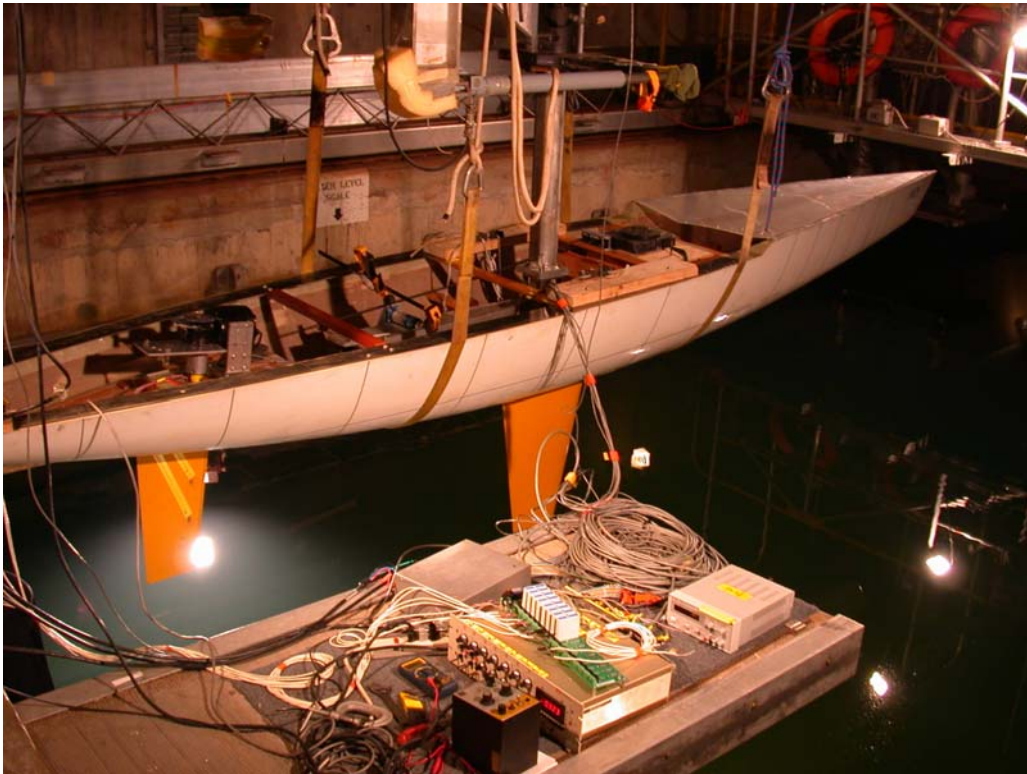


Figure 14: Model Preparation

Design of the testing matrix also allowed for maximum data collection by reducing the number and complexity of changes necessary on the model between runs. A

rudder swap was the most complicated operation, in that the model had to be lifted clear of the water, the rudder removed from the motor shaft coupling, and twenty-four different wires removed and new ones replaced. A general appreciation of the layout and procedure for these operations can be gleaned from the Figures 15 and 17 showing model preparation for a rudder swap.



Figure 15: Rudder Swap

Given these constraints, rudder swaps were generally only done at the beginning or end of the work day. Experimental conditions were arranged so that at most two but generally one of the experimental variables had to be changed between runs, proceeding from least dynamic freedom to most dynamic freedom and back down again if necessary. Since only one 0600 to 1200 working period was available for wave data collection, this

necessitated using only the low aspect ratio rudder for this portion of the testing. The irregular wave train was designed from a shallow water (JONSWAP) ocean wave spectrum. The maximum height of the waves was set so that the wave crests would

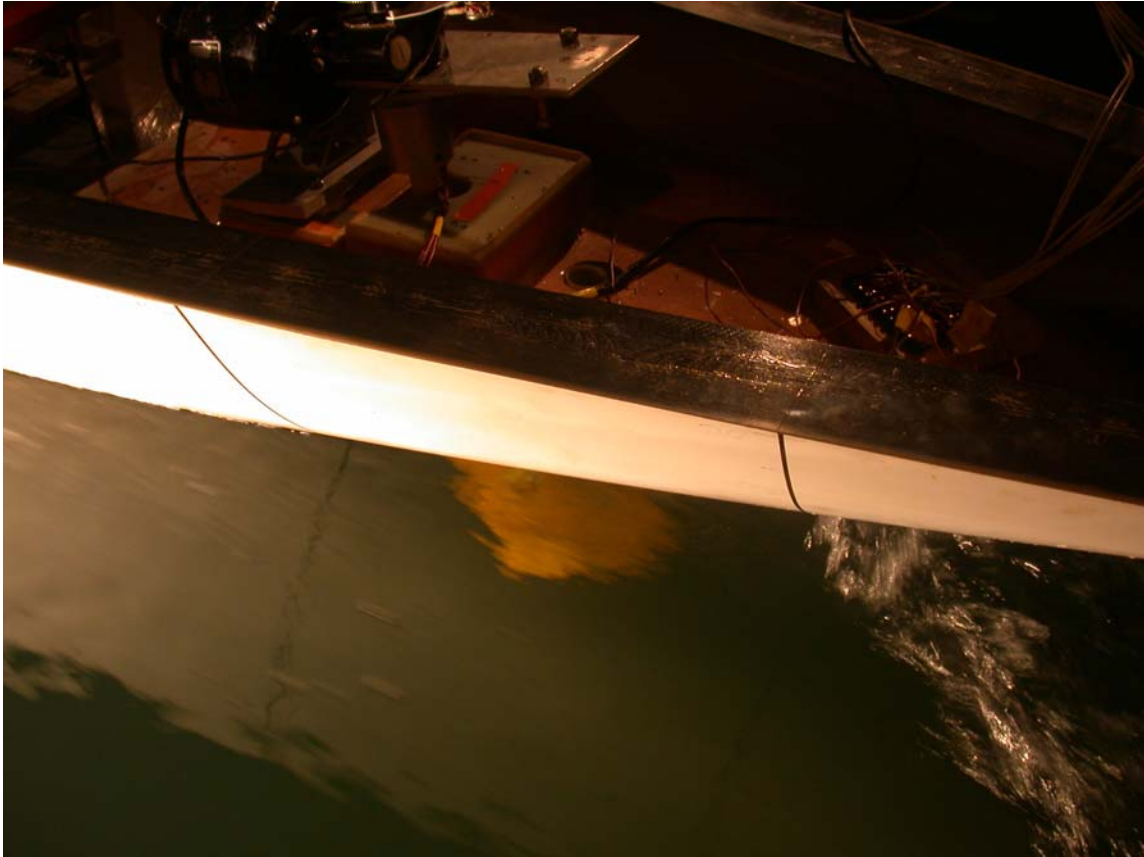


Figure 16: Flow Pattern Around Rudder—Slow Speed Test

be from one to two inches below the gunwale of the model ship giving a freeboard of fourteen inches. The modal period of the waves was then scaled so that the steepness of the waves matched the open ocean wave spectrum data.

Overall, thirty-three different towing tank runs were made allowing for the collection of four hundred and thirteen data collection cycles. Of these four hundred and thirteen samples, approximately three hundred yielded valuable data. In addition to the experimental data recorded by the electronic data collection system, the entire sequence

of tests was recorded by high resolution cameras and stored on data tapes. In addition, nearly fifty still photographs of the experimental runs were collected to aid in analysis and to present a record of the experiments conducted. What follows is a series of photographs illustrating the testing procedure.

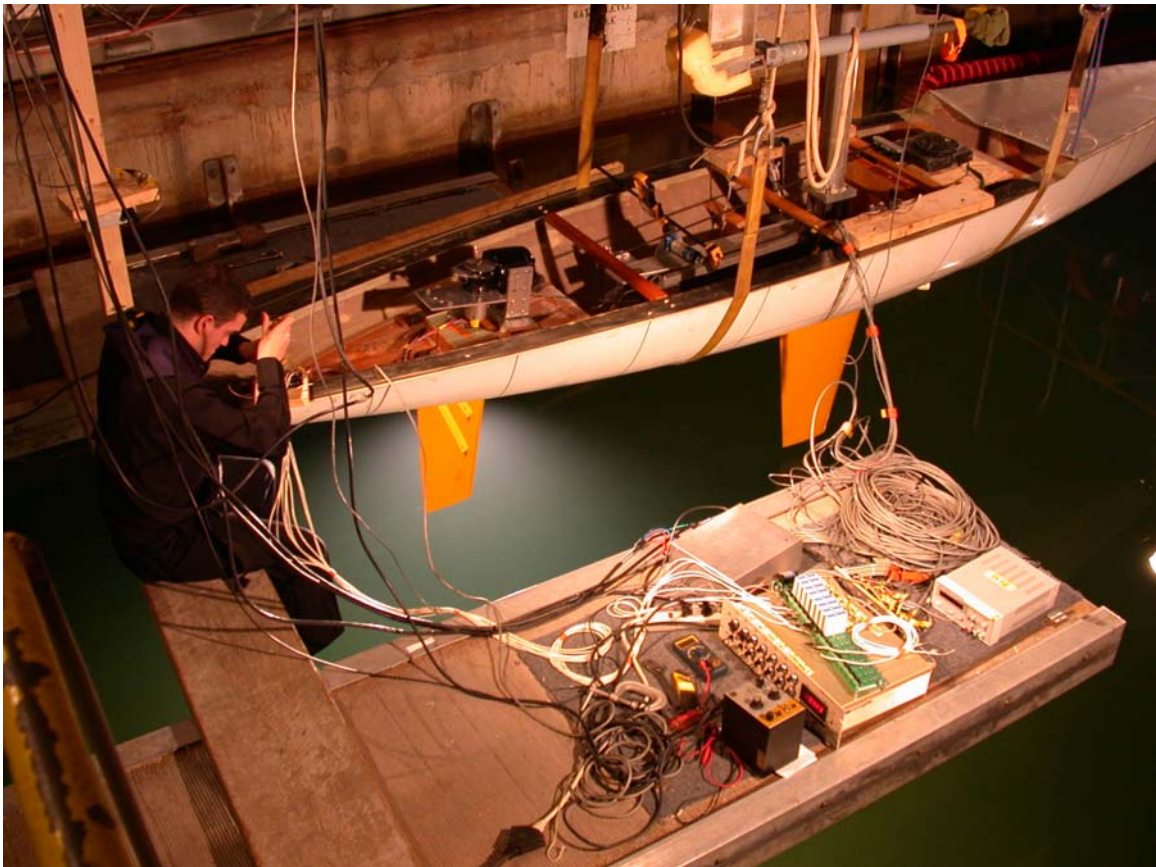


Figure 17: Rudder Swap/Equipment Layout



Figure 18: Mr. John Zselecsky, Motor Layout, and Yaw Arm/Clamp

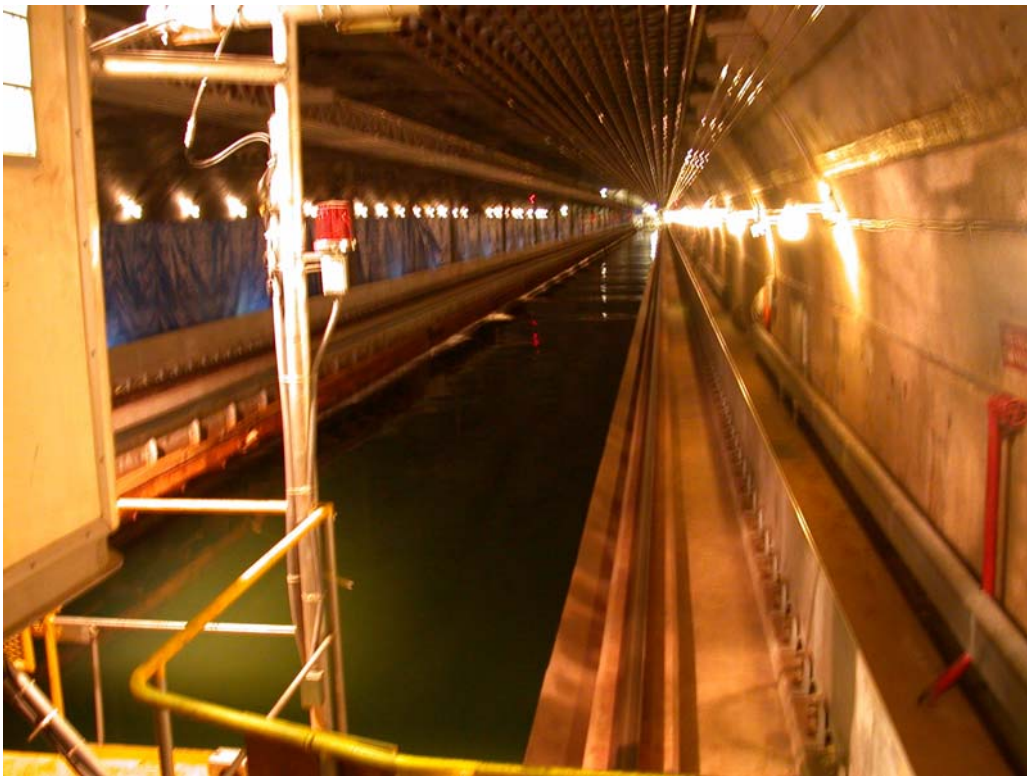


Figure 19: David Taylor Model Basin—Carriage 3



Figure 20: Towing Point, Yaw Arm, Roll, Pitch, and Yaw Pivots

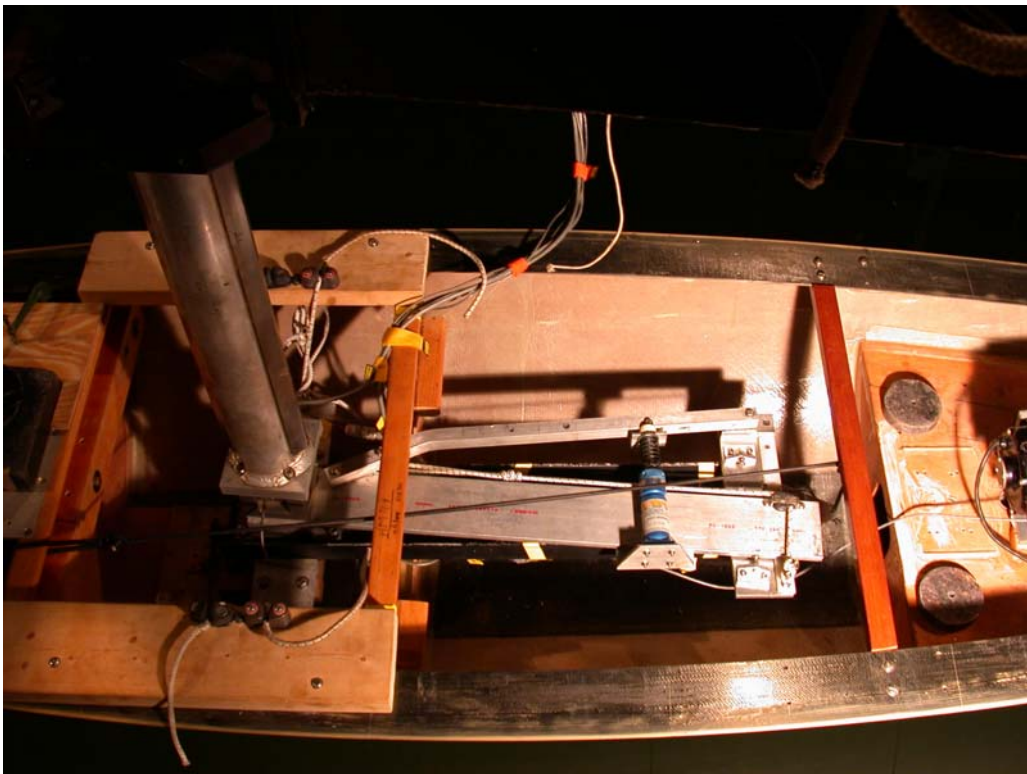


Figure 21: Towing Point, Yaw Arm, Roll Springs



Figure 22: Motor and Stop Mechanism and Rudder Gage Board



Figure 23: Yaw String



Figure 24: Carriage 3—David Taylor Model Basin Cantilever Model Jig



Figure 25: Mr. Bill Beaver Operating Rudder Angle Motor Circuit

TANK TESTING: DATA ANALYSIS METHOD

The purpose of the analysis of the experimental data collected in towing tank experimentation served to answer one question: what percentage of reduction in the loading of a rudder, and by extension the coefficient of lift, could be expected relative to the values of the coefficient of lift determined from the lift curve generated by the use of classical wing theory. In the experimental design, several parameters were analyzed so that the importance of different factors in the dynamics of the model or ship could be correlated with the loading of the rudder and so that a more accurate prediction of the loadings to be expected could be determined and more precise and efficient foil and shaft design could be accomplished.

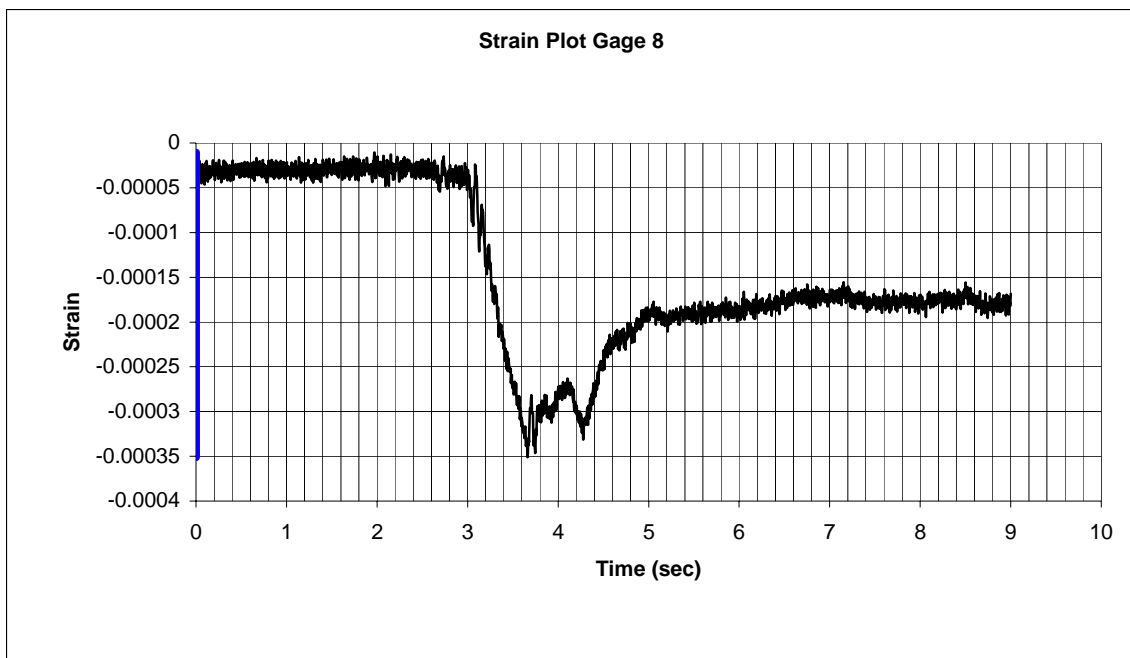


Figure 26: Sample Strain Plot for Shaft Gage

The first step of the analysis was to determine the validity of the experimental data that had been collected. Verified data plots are presented above and below to

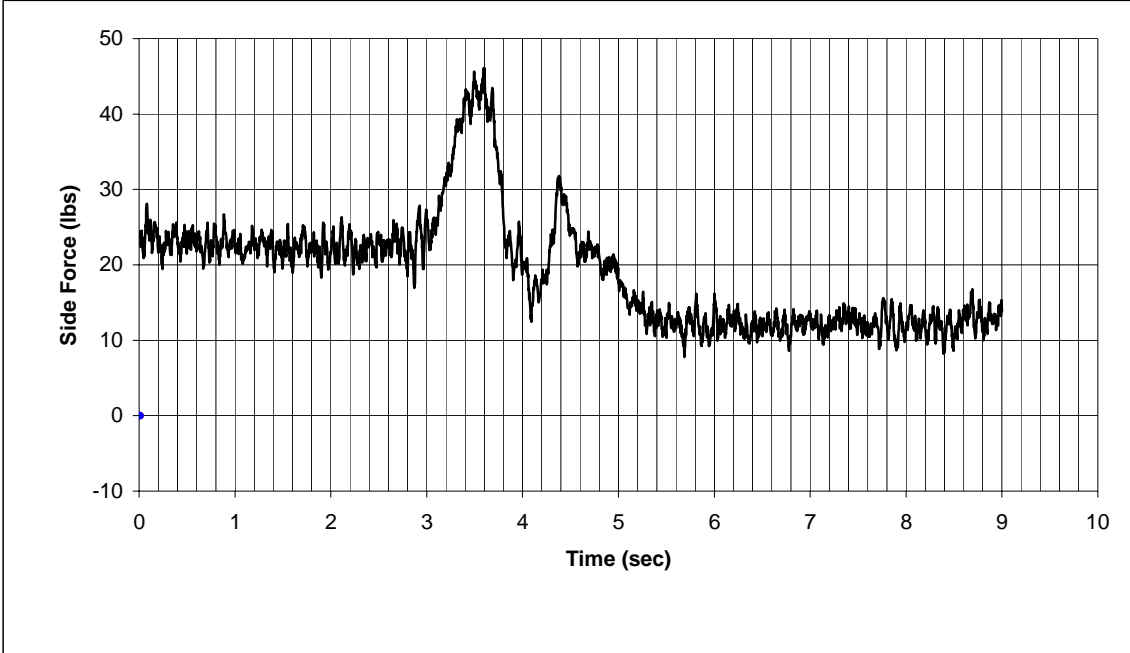


Figure 27: Sample Side Force Plot

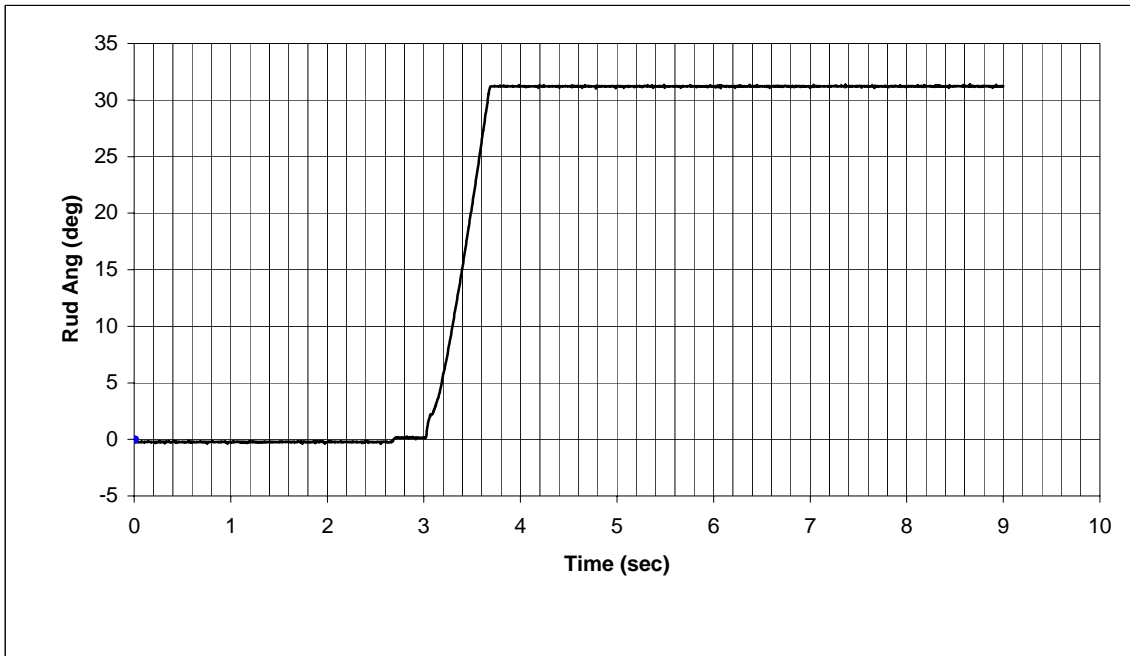


Figure 28: Sample Rudder Angle Plot

illustrate the nature of accurate readings. In order to do this, the notes taken on each of the data collection cycles, the data, and some of the video footage were analyzed and any data collection cycles that were obviously biased by factors such as operator error, malfunctions of mechanical and electrical systems, and others were eliminated from the data analysis. These types of bias included data collection cycles where the rudder shaft slipped in the coupling connecting it to the shaft of the motor, runs where the motor experienced a momentary stall and hence the rudder angle curve exhibited a pronounced step instead of a smooth straight line, runs where data was taken before the towing carriage acquired its final steady state speed, runs where multiple gages gave garbled readings, and in one occasion a situation where the signal conditioner did not have

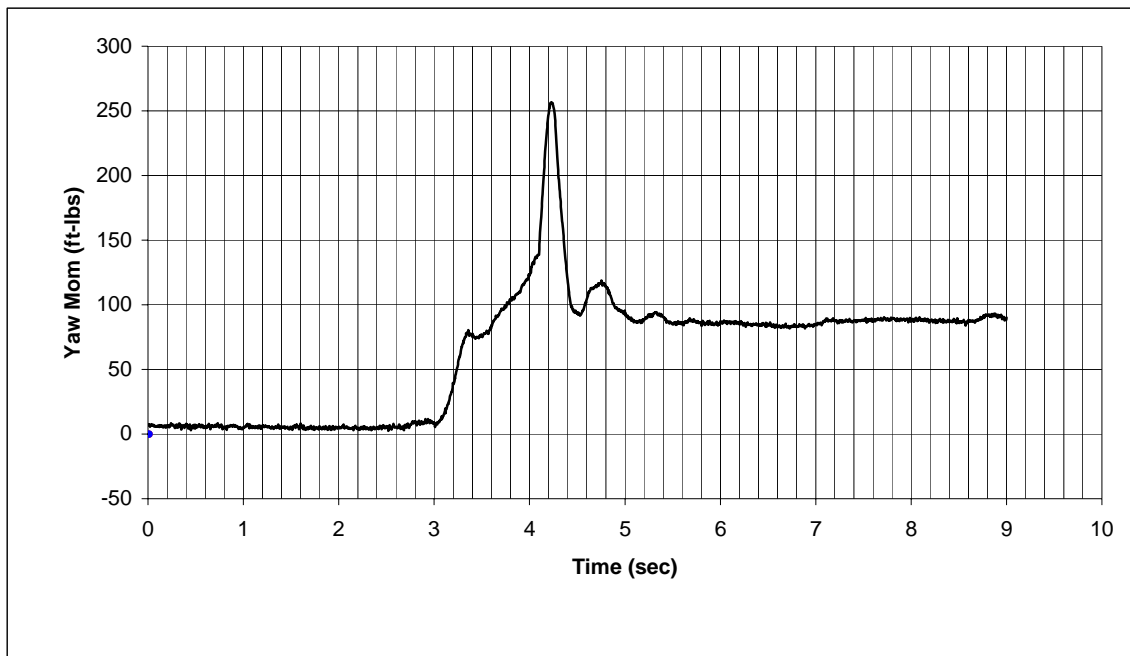


Figure 29: Sample Yaw Moment Plot

adequate power flowing through it. In addition to the elimination of erroneous experimental data collection cycles as a whole, the data acquired from several of the

channels, primarily the channels measuring rudder strain, at different points within the data collection cycles was removed from the analysis where the data was obviously suspect. These situations occurred in several instances where strain gages failed as evidenced by an extremely noisy signal with no discernable pattern. These errors were almost exclusively caused by one of three reasons. Reason one was that no power was flowing to the gages in question, either because the power supply was not operating or because one of the wires connecting the gages to the power supply had pulled loose. Because the wires passing from the gages to the power supply had to lay flush along the side of the foil, extremely thin wire was necessary to transmit both the power to and the signal from the strain gages. Given this extremely thin and fragile wire, wires often broke or pulled loose from their wire connection matrix.

The second reason for poor data in the strain gages was because of the complete failure of the strain gage itself. In only one instance did a strain gage fail completely where it was not able to be repaired or troubleshooting options explored. A continuity check with a voltmeter to establish the proper voltage reading was conducted in the model basin was generally conducted when a gage gave suspect readings and often confirmed the solution to the problem lay along the route described in reason one.

The third primary reason for bad strain data was the tank water shorting the strain gages. When the rudder was placed in water without any protective covering, the water acted as an electrical conduit short circuiting the resistance of the gage. On two occasions when continuity checks in water yielded negative results, the model was lifted from the water and a voltage continuity check applied again in air yielding positive results, the solution to the problem was found to be along these lines. A small amount of

a gelatinized silicon sealer was applied over the top of the gages to protect the gages from abrasion, to stiffen the soldered connection of the electrical wires, and to provide a protective barrier from the tank water. Since the electrical systems were the most fragile due to the massive amount of wire connection they provided the majority of the invalid data, while the robustness of the mechanical systems and their associated electrical data collection systems provided no problems.

Once the invalid data samples and data samples collected as zeroes were removed from the analysis, this left approximately three hundred different data points with a matrix of ultimately six different experimental variables to analyze.

From a simplified standpoint, the data was broken up into groups of similar testing conditions that were analyzed based on the scatter of the data for the validity. In the few instances where discrepancies existed between similar runs, extenuating factors such as the aforementioned step in the rudder rotation rate were generally the cause. In the others the scatter in the data never exceeded fifteen percent and was often found to be less than five. Since so many different variables were tested, not enough data points of each type existed to make an exhaustive analysis of the precision of the data since only approximately four data points of each type existed. This did not present a problem as the data was then reassembled into larger groups, combined and averaged with like types in order to produce data that showed a higher degree of consistency, within five percent to ten percent error. The plots of the loading versus rudder rate showed that changes in the percentage of the loading could reach twenty percent but for changes in rudder rate less than one hundred percent, the change in loading was closer to ten percent. Where the

change in rudder rate between runs met or exceeded two hundred percent, a significant increase was seen.

The main assembly of the like experimental conditions into a larger body of data comparing each dissimilar condition in turn yielded the most valuable conclusions of this project. The data was broken into two main sections by the aspect ratios of the rudders. The body of data in each of these sections was analyzed separately. The next main breakdown of the data was done by model speed. The final group breakdown of the data was done into the individual dynamic freedom conditions. The percentage change in loading due to rudder rate among the conditions was compared. These combined values were then compared in a series of plots where rudder rate and model speed were held constant. This body of data allowed for a comparison of percent reduction in loading as a function of the condition of the dynamic freedoms. In the next step an attempt was made to normalize the data by the velocity squared term in order to establish correlating trends across the velocity spectrum. This attempt at correlation gave a large standard deviation for some apparent reasons that will be discussed later in the detail section of this analysis. Finally, comparison was made between the high and a low aspect ratio rudder in order to determine what affect the aspect ratio has on the expected percent reduction of the loading of a foil.

TANK TESTING: DATA ANALYSIS RESULTS

The data analysis method described above yielded four comparisons of note. The first that will be discussed is the effect of including the dynamic freedoms of the model in the analysis versus using a static steady state analysis. The second comparison that will be discussed is the apparent effect of model velocity on the above analysis. The slow speed was a model speed of 3.04 knots, while high speed was a velocity of 5.06 knots model speed. The third comparison that will be discussed is the effect of aspect ratio of the loading. Finally, the fourth comparison that will be discussed is the effect of rudder rate on control surface loading.

Figures 30 and 31 illustrate the main conclusions derived from the analysis of

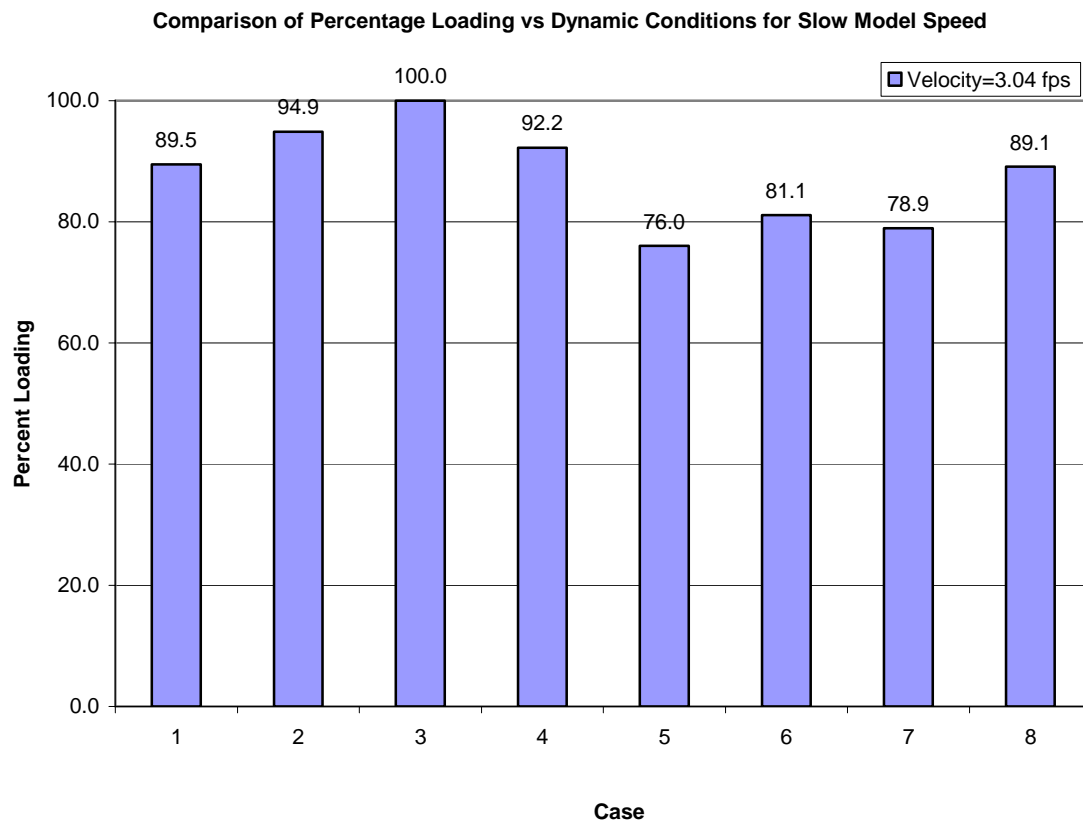


Figure 30: Rudder Loading for Slow Speed

the effect of model/ship dynamics of rudder loading. All values are normalized by the maximum values of rudder loading experienced in the experimental tests. The above plot

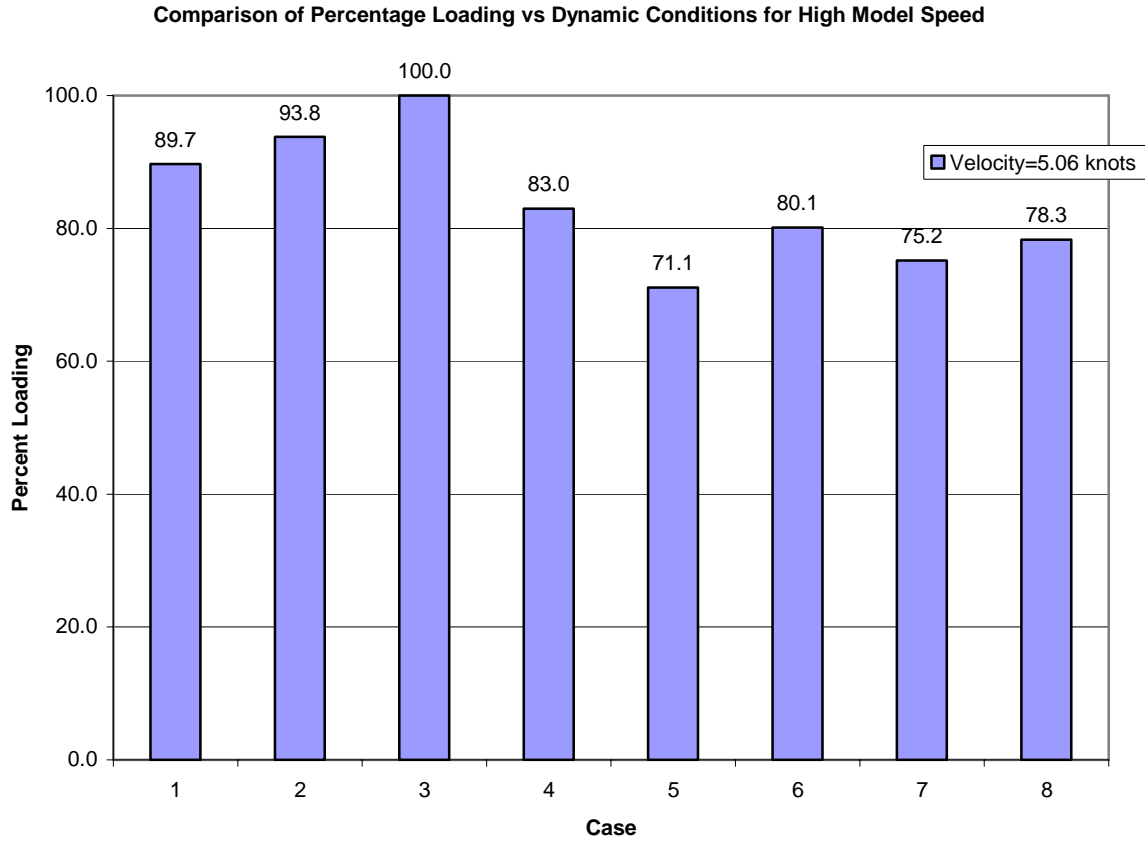


Figure 31: Rudder Loading for High Speed

gives relative magnitudes of the reduction in rudder loading that one would expect given the dynamic conditions. In each case, the values listed in Figures 30 and 31 are in

Testing Matrix	
Case 1:	Fixed 5 Degrees Yaw/Free Roll
Case 2:	Fixed 5 Yaw/Fixed Roll
Case 3:	Fixed 5 Degrees Yaw/Fixed Roll
Case 4:	Fixed Zero Yaw/Fixed Roll
Case 5:	Free Yaw/Roll Damping
Case 6:	Fixed Zero Yaw/Free Roll
Case 7:	Free Yaw/No Roll Damping
Case 8:	Low Aspect Ratio Rudder in Waves

Table 2: Model Basin Testing Matrix

order from Case 1 to Case 7 left to right. The different cases are reproduced as a key to case descriptions in Table 2 above. The values represent the average of both rudders except for Case 8 which describes only the low aspect ratio rudder.

The biggest factor in the amount of reduction in loading is due to the energy dissipated in allowing the vessel to yaw through its range of motion during the transient phase of a turning maneuver. Freedom in yaw reduced the loading in the rudder shaft by roughly ten to twenty-five percent. Freedom in roll, on the other hand, reduced the loading in the shaft by only five to ten percent for the slow speed case. Damping the oscillations of the model reduced expected loading by three percent, leading to the conclusion that including the dissipation energy through roll stabilization in calculations can further reduce the force that would otherwise be expected to move through the load paths in the rudder shaft.

The key result of this analysis, however, is the percent reduction that can be expected in rudder shaft loading for a vessel performing a maneuver statically versus dynamically. For a vessel allowed to oscillate about all of its major axes (i.e. the model was permitted to pitch, roll, and yaw), the reduction for the low speed case was nearly twenty-five percent.

For the higher speed values, the percent reduction in loading followed the trends described above as shown in Figure 31, except in the cases involving freedom in roll. There the percent reduction in loading was between three to six percent less than that experienced in the slow speed case.

DATA ANALYSIS: FINITE ELEMENT ANALYSIS RESULTS

The final step of this rudder analysis was to take the loading data for the two rudders of different aspect ratios and derive the actual values of the dynamic lift coefficient through the use of the finite element model developed for each of the rudders. In order to achieve this end, the assumed pressure distribution for the rudder was developed using a computational fluid dynamics program named X-Foil. Using this distribution of the pressure across the span and the chord of the rudder, the magnitude of the pressures was varied iteratively, while maintaining the same relative distribution, until the final values for the strain due to the assumed pressures applied to the finite element model matched the experimental strains observed in the towing tank data. By using this method of analysis, the lift coefficients were extracted from the experimental data along all of the sections of the rudder so that the results as applied to the particular designs of rudder chosen can be applied universally to all rudder designs of similar composition.

The objective described above was accomplished by adapting the theoretical pressure distribution given for a NACA 0012 foil.⁶ The “00” at the beginning of the foil designation indicates that it is symmetrical about the plane running longitudinally through the rudder. The “12” at the end of the foil designation indicates that the maximum thickness of the foil is twelve percent of the foil’s chord length. Both of the rudders used a twelve percent foil thickness through the entire lengths of the rudder span simplifying the analysis. The shape of the theoretical pressure distribution along the chord of the foil was used, with the assumption that the span wise component of the lift along the surface of the foil remained constant until the flow effects around the tip of the foil reduced the effective pressure at the end. With this assumed shape of the pressure distribution around the foil

scaled as a function of the maximum expected pressure, the total pressure on the surface of the rudder blade was adjusted by scaling the maximum pressure, until the experimental strains measured during the data analysis phase of the tank testing matched the theoretical strains. Shown below are the resulting strains from the high aspect ratio rudder model under its pressure load. Inserting several different iterations of pressure distributions into

L1n STRAIN Lc=1

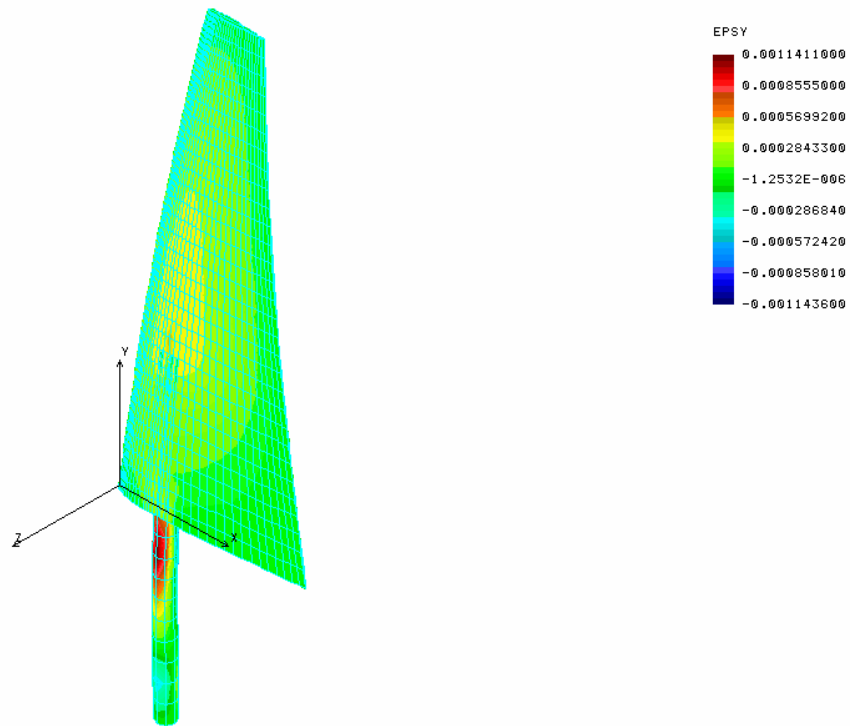


Figure 32: High Aspect Ratio Strain Plot—High Speed

the finite element model developed the theoretical strains. The finite element model calculated the stresses and strains present at each element and each node comprising the two rudders. Of particular interest were the theoretical strains developed at a point one inch above the rudder blade on the shaft, and at six and twelve inches below the root of the foil, as these were the locations of the strain gages. The pressures against each element of the

composite laminate on the surface of the rudder were adjusted until the resultant strains at the locations of interest matched the experimental data set values.

Once the proper pressure distributions had been applied to the two finite element models, and output data was found to be satisfactory, the maximum pressure and mean pressure for each condition were extracted from the model data. The mean pressure was then inserted into equation (1), along with the values for velocity and density of fresh water in order to derive the mean coefficient of lift for the body. Using the assumed pressure distribution, and the mean pressure, the scaled pressure at any point along the body can be calculated. Coefficients of lift were derived for each of the rudders at the lower and higher speeds respectively. The specific cases investigated were the model data sets where the model was allowed to oscillate in all degrees of freedom, but was damped in roll. The values for the dynamic lift coefficient in the other cases can be approximated through the table of percent reduction in lift given earlier in this report for the respective rudder aspect ratios and model speeds. These cases investigated were most specifically of interest because their dynamics most represented the dynamics of a vessel at sea, and also gave the greatest reduction in lift coefficient compared with the full-scale theoretical value for lift.

These dynamically free values of lift were compared with the theoretical maximum value of lift coefficient for the respective rudders and also with a test done quasi-statically as the model was towed down the tank. In the quasi-steady test, the model was held at zero degrees yaw and the rudder was varied in five degree increments. This developed an experimental strain curve with a peak well below the peak seen in the dynamic tests. The theoretical maximum coefficient of lift for both rudder sections was approximately 1.6.

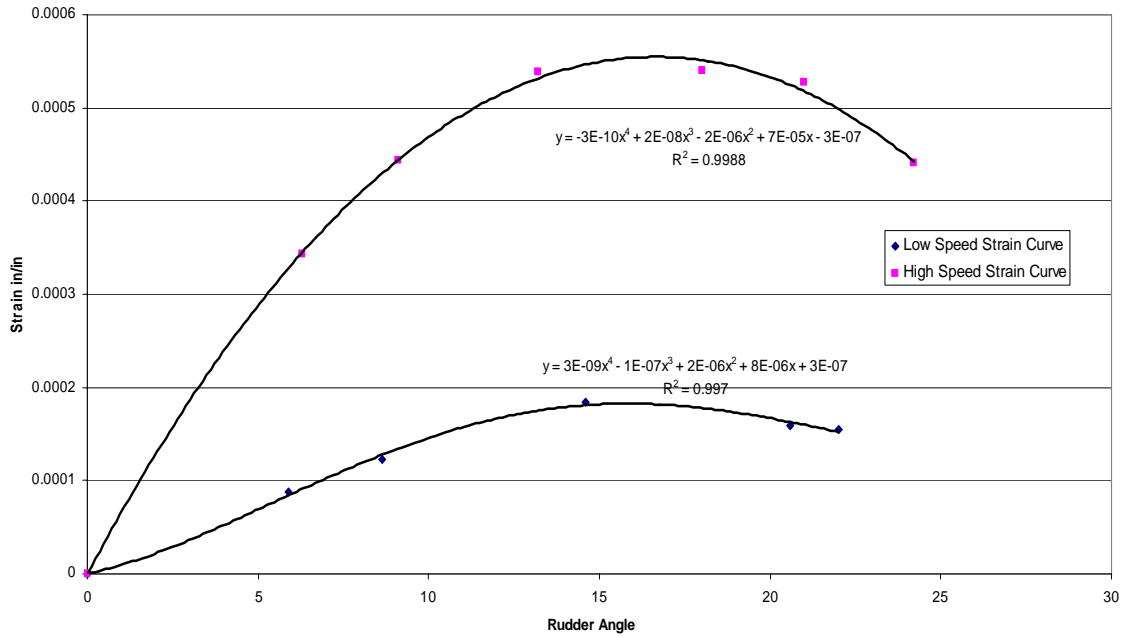


Figure 33: High Aspect Ratio Rudder Static Loading Curve

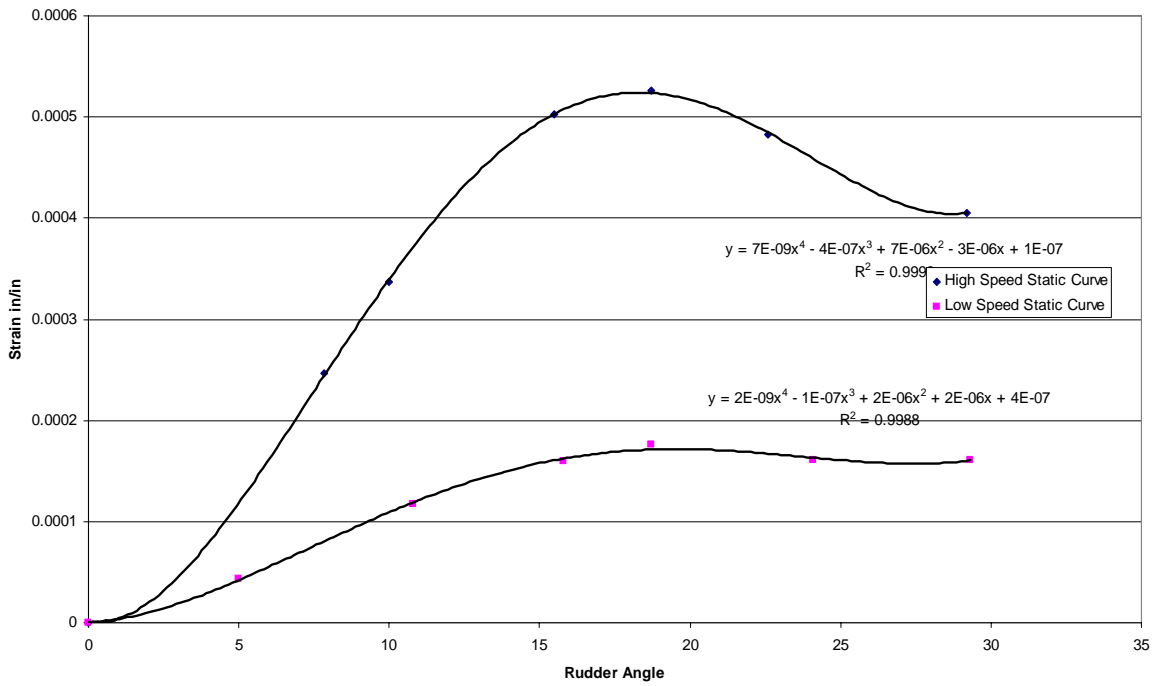


Figure 34: Low Aspect Ratio Rudder Static Loading Curve

Therefore, all experimental values fell well below the theoretical maxima. The strain curves for the high and low aspect ratio rudders are shown in Figures 33 and 34.

The results of the pressure-strain correlation are listed in the Tables 3 and 4. In each case the maximum pressure, mean pressure, and mean coefficient of lift for the foil in question are presented and clearly marked. The speeds are listed in feet per second, the pressures are in pounds force per square foot, and the dynamic lift coefficients in all cases are dimensionless.

High Aspect Ratio Rudder				
Speed	5.13	fps	8.54	fps
Strain	0.000351		0.001051	
Maximum Pressure	0.294	psi	0.743	psi
Maximum Pressure	42.34	psf	107	psf
Mean Pressure	0.208	psi	0.527	psi
Mean Pressure	30	psf	75.9	psf
Dynamic Lift Coefficient	1.17		1.07	
Static Maxima				
Strain	0.000174		0.000556	
Lift Coefficient	0.58		0.566	
Case 1	1.38		1.24	
Case 2	1.46		1.29	
Case 3	1.54		1.38	
Case 4	1.42		1.14	
Case 5	1.17		0.98	
Case 6	1.25		1.10	
Case 7	1.21		1.04	

Table 3: High Aspect Ratio Rudder Data

Low Aspect Ratio Rudder				
Speed	5.13	fps	8.54	fps
Strain	0.000303		0.0007	
Maximum Pressure	0.284	psi	0.701	psi
Maximum Pressure	40.9	psf	100.9	psf
Mean Pressure	0.21	psi	0.496	psi
Mean Pressure	30.2	psf	71.4	psf
Dynamic Lift Coefficient	1.19		1.01	
Static Maxima				
Strain	0.000172		0.000531	
Lift Coefficient	0.675		0.767	
Case 1	1.37		1.17	
Case 2	1.46		1.22	
Case 3	1.53		1.30	
Case 4	1.41		1.08	
Case 5	1.17		0.93	
Case 6	1.24		1.04	
Case 7	1.21		0.98	
Case 8	1.36		1.02	

Table 4: Low Aspect Ratio Rudder Data

In each case the low speed coefficient of lift was greater than the higher speed coefficient of lift. Theoretically the pressure distribution applied to each of the rudders should vary as the square of the velocity. In this case, however, the change in the scaled pressures falls below the expected value. At the higher speeds, the model began to ventilate. This is one explanation for the drop in dynamic lift coefficient. In a perfect fluid, i.e., a fluid without viscosity, and absent a free surface, the lift curve should match the theoretical curve. In this case, however, the foil approached the free surface interface between the tank water and the surrounding air. As a result, air was sucked into a cavity on the back (non-pressure) side of the foil, thereby relieving some of the pressure. The photographs and film record of the tank testing show this to be occurring. The difference between the higher and lower aspect ratio models matches roughly with what is expected

from classical wing theory. The higher aspect ratio exhibits a six percent increase in the lift coefficient. As evidenced by the strain plots, however, the loading in the rudder shaft due to the greater bending moment caused by the longer foil is nearly twice as great in the higher aspect ratio rudder as in the lower aspect ratio rudder.

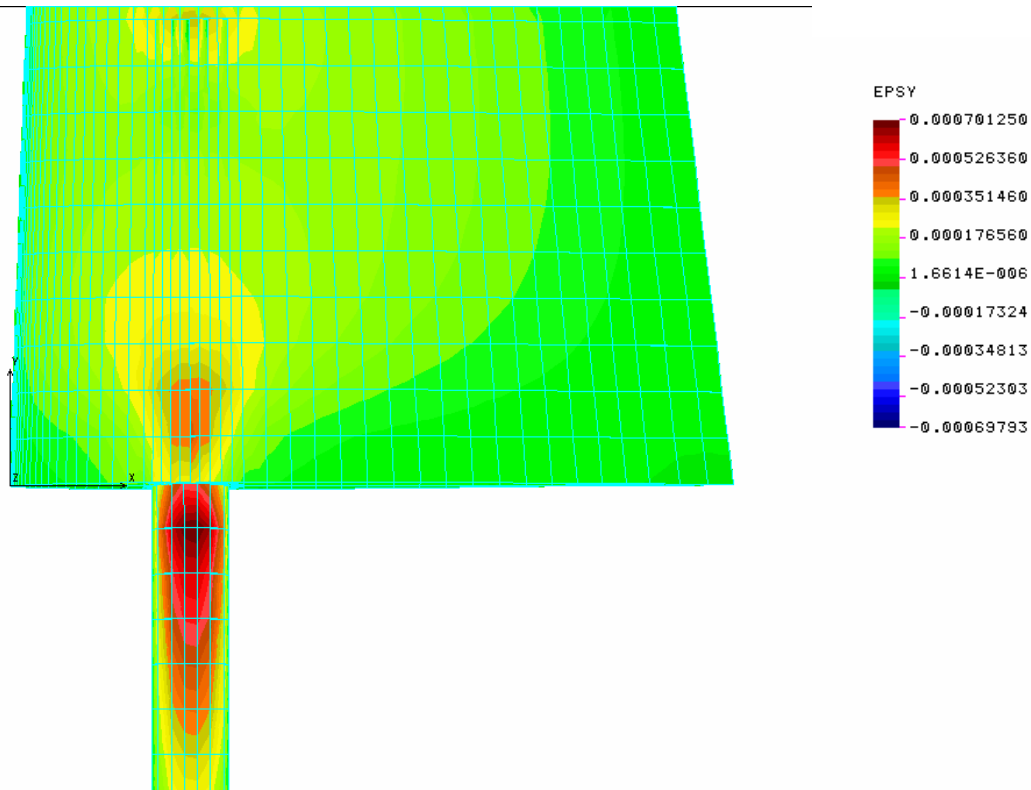


Figure 35: High Aspect Ratio Rudder Shaft Strain Plot

In both cases the rudders were constrained in translational motion at the surface nodes on the top two inches of the shaft, where the shaft was inserted into the motor shaft coupling. In addition, the outer surface nodes of the rudder shaft were constrained from moving laterally in either direction at the joint of the rudder shaft and the root of the foil. This was the location where the rudder shaft was constrained by the bearing attached to the bottom of the vessel hull. In both models the shaft was unconstrained in the vertical, or y,

direction, as the bearing in the hull provided negligible (frictional) constraint to vertical motion of the rudder and shaft structure.

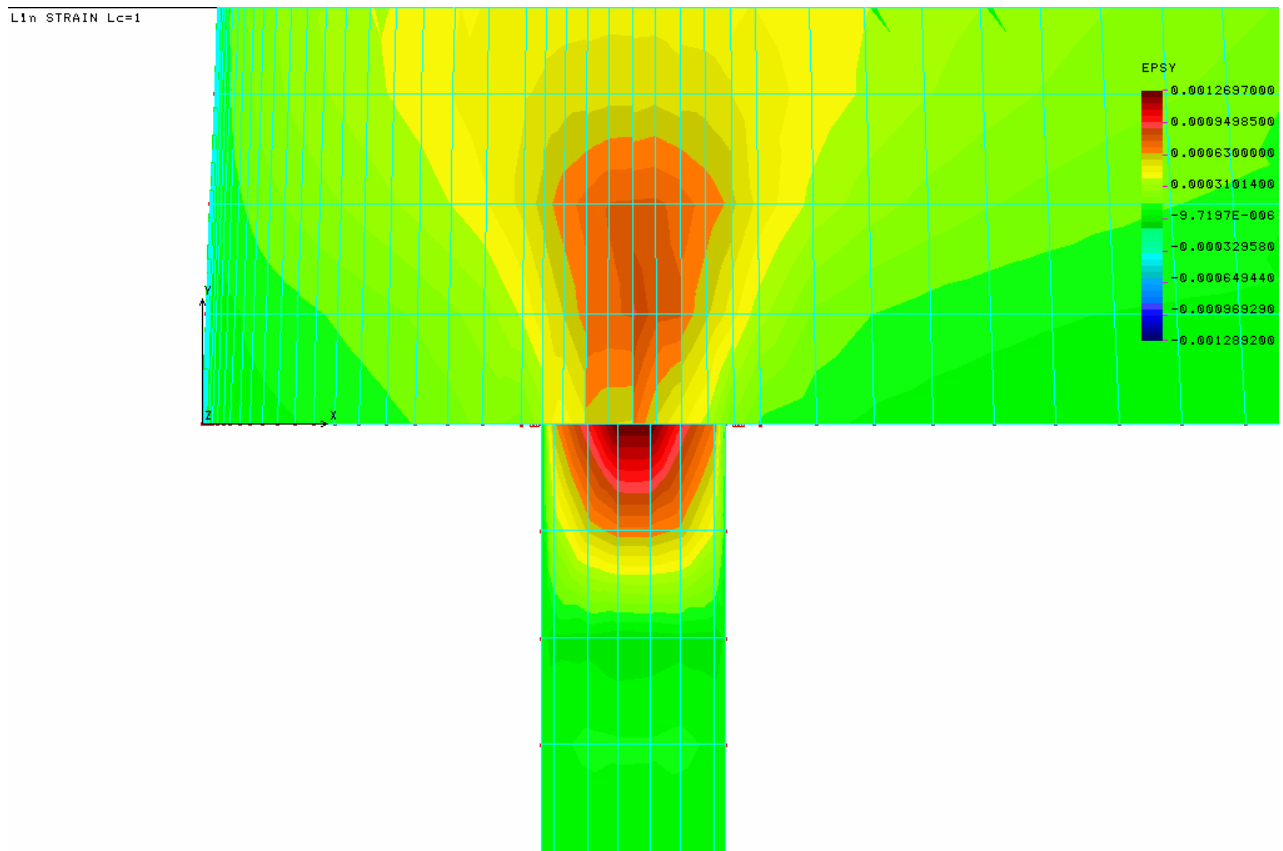


Figure 36: Low Aspect Ratio Rudder Shaft Strain Plot

CONCLUSION

The American Bureau of Shipping requires shipbuilders to design to the theoretical maximum lift coefficients. In this study the maximum lift coefficients for the most realistic case were recorded as 19.3% below the theoretical maximums. The dynamic runs did produce maximum values for the lift coefficient, 24-43% higher than the quasi-static. Only in the most unrealistic condition, with the model held at a constant yaw angle with no ability to turn, did the values for the lift coefficient exceed the American Bureau of Ships mandated coefficient of 1.5. The conclusion of this report is that although dynamic effects were present in the experimental testing, they did not cause a peak value for the dynamic lift coefficient that exceeded the design values in the realistic test conditions. The cause of the rudder failures did not appear to be due to underestimation of the loads.

RECOMMENDATIONS FOR FURTHER STUDY

The conclusion of this project opens up a wealth of opportunities for research in this field. Literature on the subject is limited, indicating little prior research on effect of dynamics on rudder performance. This investigation touched the surface of the subject. Many different variables were examined, but due to the limited scope of the project, the depth of the examination did not give the topic justice. Use of a more realistic model for the dynamics of a real ship presents possibilities for investigation, as does the use of a completely similar dynamic model in a maneuvering basin. More research is also needed in the areas covered by this report. Due to the fact that four or five different variables were analyzed on each testing run, the number of repeated tests was not sufficient to make an adequate statistical analysis on the repeatability of the data.

The correlation of experimental data to theoretical fluid dynamics programs is also a very exciting prospect. In this project, only one data sample was compared to the theoretical loads developed from a computational fluid dynamics program, and a simplified, upright, quasi-steady analysis. The involvement of more sophisticated software increasingly available to the industry makes the modeling of the more complicated dynamic problems analyzed in the experimental phase of this investigation a real possibility. Hopefully this report will peak interest in this field of research.

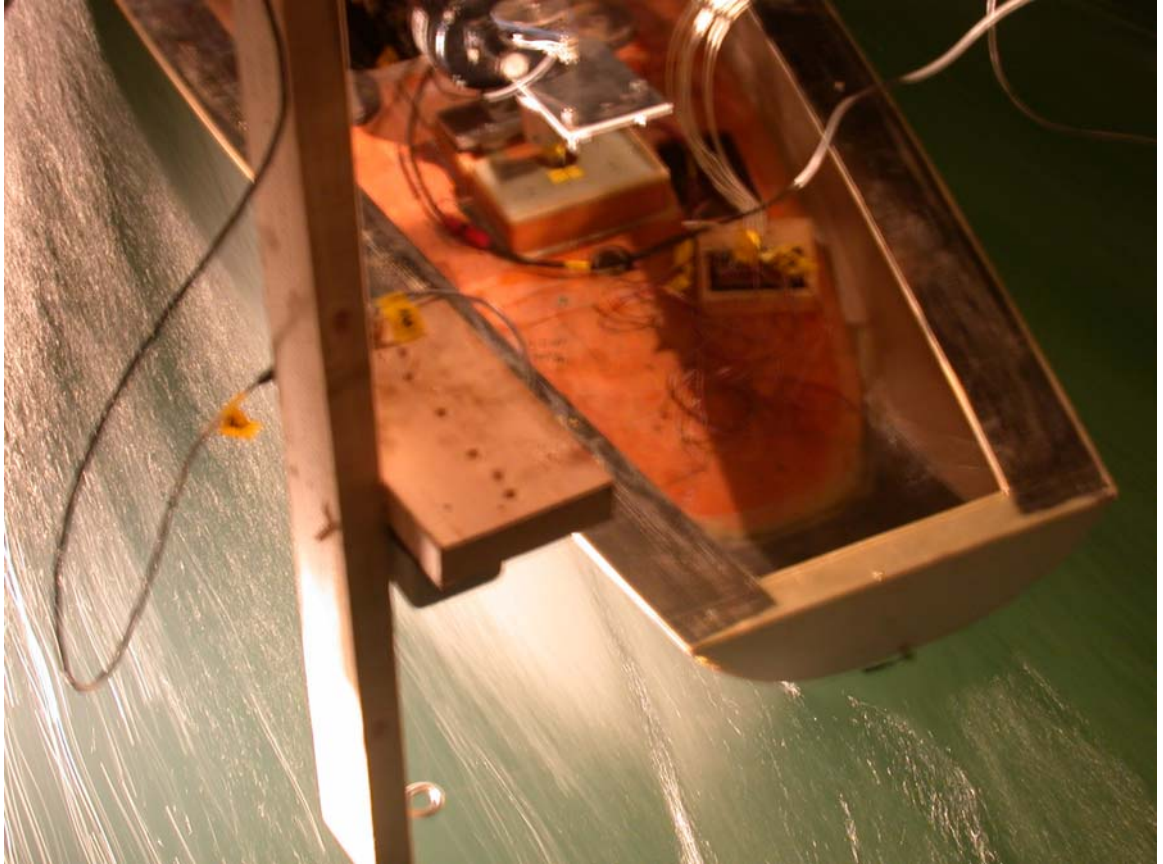


Figure 37: The End

ENDNOTES

¹ Killing, Steve and Douglas Hunter. Yacht Designing Explained: A Sailor's Guide to the Principles and Practices of Design. New York: W.W. Norton & Co, Inc, 1998, 111.

² Killing, 111

³ Mott, Lawrence V. The Development of the Rudder. London: Chatham, 1997, 47.

⁴ Killing, 117-18.

⁵ Lewis, Edward V., ed. Principles of Naval Architecture. 3 vols. Jersey City: Society of Naval Architects and Marine Engineers, 1989, 209-10.

⁶ Abbott, 305.

BIBLIOGRAPHY

- COSMOSM 2.8 (64K Version) April 2003. Structural Research and Analysis Corporation: Los Angeles.
- Figliola, Richard S. and Donald E. Beasley. Theory and Design for Mechanical Measurements. New York: John Wiley & Sons, 1991.
- Killing, Steve and Douglas Hunter. Yacht Designing Explained: A Sailor's Guide to the Principles and Practices of Design. New York: W.W. Norton & Co, Inc, 1998.
- Larsson, Lars and Rolf E. Eliasson. Principles of Yacht Design. Blacklich: McGraw-Hill, 2000.
- Leechman, G.F. The Practice and Theory of Steering. Glasgow: James Brown & Sons, 1927.
- Lewis, Edward V., ed. Principles of Naval Architecture. 3 vols. Jersey City: Society of Naval Architects and Marine Engineers, 1989.
- Mott, Lawrence V. The Development of the Rudder. London: Chatham, 1997.
- Ottosen, Niels Saabye and Hans Petersson. Introduction to the Finite Element Method. New York: Prentice Hall, 1992.
- Sirohi, R.S. and H.C. Radha Krishna. Mechanical Measurements. New York: John Wiley & Sons, 1991.
- Stoekert, J. and H. Gatzer. "Hydrodynamic Loads on the Rudder of a Ship Travelling in Regular Waves." Schiffbauforschung. 27 (1988): 38.